A global simulation of brown carbon: Implications for photochemistry and direct radiative effect

D. S. Jo[1], R. J. Park[1,*], S. Lee[1], S.-W. Kim[1], and X. Zhang[2]

[1]{School of Earth and Environmental Science, Seoul National University, Seoul, 151-747, Republic of Korea}

[2]{Department of Civil and Environmental Engineering, University of California, Davis, CA, USA}

Correspondence to: R. J. Park (rjpark@snu.ac.kr)

Abstract

Recent observations suggest that a certain fraction of organic carbon (OC) aerosol effectively absorbs solar radiation, which is also known as brown carbon (BrC) aerosol. Despite much observational evidence of its presence, very few global modeling studies have been conducted because of poor understanding of global BrC emissions. Here we present an explicit global simulation of BrC in a global 3-D chemical transport model (GEOS-Chem), including global BrC emission estimates from primary (3.9 ± 1.7 and 3.0 ± 1.3 TgC yr^{-1} from biomass burning and biofuel) and secondary (5.7 TgC yr^{-1} from aromatic oxidation) sources. We evaluate the model by comparing the results with observed absorption by water-soluble OC in surface air in the United States, and with single scattering albedo observations at AERONET sites all over the globe. The model successfully reproduces the observed seasonal variations, but underestimates the magnitudes, especially in regions with high secondary source contributions. Our global simulations show that BrC accounts for 21% of the global mean OC concentration, which is typically assumed to be scattering. We find that the global direct radiative effect of BrC is nearly zero at the top of the atmosphere, and consequently decreases the direct radiative cooling effect of OC by 16%. In addition, the BrC absorption leads to a general reduction of NO_2 photolysis rates, whose maximum decreases occur in Asia up to -8% (-17%) on an annual (spring) mean basis. The resulting decreases of annual (spring) mean surface ozone concentrations are up to -6% (-13%) in Asia, indicating a non-negligible effect of BrC on photochemistry in this region.

47 ## 1 Introduction

48 Carbonaceous aerosols (CAs) are one of the poorly understood aerosols (Goldstein
49 and Galbally, 2007; Park et al., 2003) and are divided into black carbon (BC) and organic
50 carbon (OC) aerosols. These two types of CAs are emitted together mainly by combustion
51 processes (except for secondary organic carbon, SOC). In the literature, BC is considered as
52 light-absorbing and OC as light-scattering aerosols until recently. Therefore, the climatic
53 effect of CAs depends on the relative contributions of BC to CAs. For example, the net direct
54 radiative forcing (DRF) of biomass burning is estimated to be negligible, whereas diesel use
55 causes climate warming although the first source is larger than the latter for CAs (Forster et
56 al., 2007).

57 Many field observations and chamber studies recently showed that a certain fraction
58 of OC could absorb solar radiation, especially for ultra-violet wavelengths (< 400 nm)
59 (Alexander et al., 2008; Hecobian et al., 2010; Kirchstetter and Thatcher, 2012; Kirchstetter
60 et al., 2004; Yang et al., 2009). This light-absorbing OC fraction is referred to as brown
61 carbon (BrC) aerosol (Andreae and Gelencser, 2006; Laskin et al., 2015). If BrC is prevalent,
62 and its DRF is significant, then previous estimates of the DRF of CAs need to be revised.

63 Recent studies showed that the solar absorption of BrC is not negligible, and is even
64 comparable to that of BC (Alexander et al., 2008; Chung et al., 2012; Kirchstetter and
65 Thatcher, 2012). Using residential wood smoke samples, Kirchstetter and Thatcher (2012)
66 calculated that BrC absorption accounts for 14% of total solar absorption by CA, and even
67 contributes 49% of solar absorption of CA at wavelengths below 400 nm. Chung et al. (2012)
68 found that OC contributes about 45% of CA absorption at 520 nm by analyzing observations
69 at the Gosan site in South Korea. Using aerosol optical property observations at Aerosol

70 Robotic Network (AERONET) sites, Bahadur et al. (2012) estimated that BrC absorption at
71 440 nm is about 40% of BC absorption at the same wavelength, whereas at 675 nm it is less
72 than 10% of BC absorption.
73 Several efforts have also been made to examine the chemical and physical properties
74 of BrC. Some studies showed that humic-like substances (HULIS) were related to BrC
75 (Hoffer et al., 2006; Kim and Paulson, 2013; Lukács et al., 2007) based on the high
76 absorption Ångström exponent (AAE) of HULIS in the range of 6–7, indicating that the
77 specific absorption increases substantially towards the shorter wavelengths (Hoffer et al.,
78 2006), although the sources and the dominating chromophores of HULIS have not clearly
79 been revealed yet (Moise et al., 2015; Graber and Rudich, 2006). Alexander et al. (2008)
80 observed individual BrC spheres in East Asian outflows, and showed that the characteristics
81 of BrC spheres (AAE of 1.5) were different from those of HULIS and also strongly
82 absorbing. On the other hand, several classes of compounds have been identified as potential
83 contributions to BrC - nitroaromatic compounds, such as nitrophenols, imidazole-based and
84 other N-heterocyclic compounds, and quinones (Laskin et al., 2015). Furthermore, SOC
85 produced from aromatic species has been found to absorb solar radiation, especially in high
86 NOx conditions (Jaoui et al., 2008; Laskin et al., 2015; Lin et al., 2015; Liu et al., 2012;
87 Nakayama et al., 2010; Nakayama et al., 2013; Yu et al., 2014; Zhong and Jang, 2011).
88 Even though the chemical composition of BrC is not clearly understood yet,
89 observations strongly indicate possible important sources of BrC (Laskin et al., 2015). Using
90 the positive matrix factorization analysis of absorption at 365 nm over the southeastern
91 United States in 2007, Hecobian et al. (2010) showed that biomass burning was the most
92 dominant source of BrC (55%), followed by SOC (26-34%). Many other studies have also

93 suggested biomass burning as the most important BrC source (Chakrabarty et al., 2010;
94 Clarke et al., 2007; Favez et al., 2009; Hoffer et al., 2006; Kirchstetter and Thatcher, 2012;
95 Kirchstetter et al., 2004; McMeeking, 2008; Saleh et al., 2014). Several studies recently
96 proposed SOC as an additional BrC source, especially when it is aged in the atmosphere
97 (Bones et al., 2010; Flores et al., 2014; Hawkins et al., 2014; Jaoui et al., 2008; Laskin et al.,
98 2014; Laskin et al., 2010; Liu et al., 2014; Nakayama et al., 2010; Nakayama et al., 2013;
99 Nguyen et al., 2012; Updyke et al., 2012; Zhang et al., 2011; Zhong and Jang, 2011).
100 Despite the ample observational studies, very few modeling studies have been
101 conducted to simulate global and regional distributions of BrC and to further quantify its
102 radiative effect (Feng et al., 2013; Jacobson, 2001; Lin et al., 2014; Park et al., 2010; Wang et
103 al., 2014). Jacobson (2001) first assumed 10% of OC as a solar-absorbing aerosol in a model,
104 and this assumption resulted in an increase of the global DRF by 0.03–0.05 W m^{-2}. Park et al.
105 (2010) estimated BrC concentrations in East Asia using the mass ratio of BrC to BC, and the
106 resulting annual clear-sky DRF of BrC over East Asia was 0.05 W m^{-2}. Feng et al. (2013)
107 simulated global BrC concentrations by considering 92% of OC from biomass burning and
108 biofuel use as BrC, and estimated 0.09 W m^{-2} for the global clear-sky DRF of BrC. Lin et al.
109 (2014) calculated the DRF of OC by assuming that all of the biomass burning and the biofuel
110 OC is BrC, and all of the SOC (as a high-absorbing case) as BrC. They estimated the global
111 clear-sky DRF of OC as -0.20 W m^{-2}.
112 In this study, we estimate global primary BrC emissions from open burning and
113 biofuel use based on a reported relationship between AAE and modified combustion
114 efficiency (MCE) (McMeeking, 2008). In addition to the primary source above, we also
115 consider SOC produced from aromatic oxidation as a secondary source of BrC (Hecobian et

al., 2010; Jaoui et al., 2008; Lin et al., 2015; Nakayama et al., 2010; Nakayama et al., 2013; Zhong and Jang, 2011). Based on these sources, a global distribution of BrC concentrations is explicitly simulated for the entire year of 2007 using a global 3-D chemical transport model (GEOS-Chem). We evaluate the model by comparing its results with observations in the United States and all over the globe. Using the best estimate of annual mean BrC concentrations, we examine the global direct radiative effect (DRE) of BrC and its effect on photochemistry.

2 BrC emissions

In this section, we discuss our method to estimate primary and secondary sources of BrC, and provide explicit global BrC emissions. The primary and secondary sources include biomass burning and biofuel use, and the production from aromatic volatile organic compounds (VOCs), respectively. Estimated global emissions are used as input for GEOS-Chem below to explicitly simulate spatial and temporal distributions of BrC concentrations.

2.1 Primary sources

Biomass burning is the largest source of CA aerosols globally (Bond et al., 2004). OC is primarily emitted during the smoldering (low-temperature burning) phase of combustion (Chakrabarty et al., 2010; Chakrabarty et al., 2014; Schnaiter et al., 2006), whereas BC is preferentially emitted from the flaming (high-temperature burning) phase. Therefore, BrC is also emitted largely during the smoldering phase of burning. Here we use the relationship between the burning efficiency and the observed aerosol light absorption to estimate the BrC emission from biomass burning.

Previous studies have suggested MCE defined in Eq. (1) below to provide

quantitative information of burning efficiencies that can be categorized into flaming versus smoldering combustion (Kaufman et al., 1998; Ward et al., 1992; Ward and Hao, 1991). For example, Reid et al. (2005) used a MCE value of 0.9 to differentiate between flaming (MCE > 0.9) and smoldering combustion (MCE < 0.9).

$$\mathrm{MCE} = \frac{\Delta C_{CO_2}}{\Delta C_{CO_2} + \Delta C_{CO}}, \quad (1)$$

where ΔC is the change in species concentration in fire off-gas relative to clean air [molecules m^{-3}].

McMeeking (2008) further found a linear relationship between the observed attenuation Ångström exponents and the calculated MCE values from a number of biomass burning samples, as shown in Eq. (2).

$$\mathring{A} = -17.34 \times \mathrm{MCE} + 18.20, \quad (2)$$

where Å is the AAE of biomass burning samples.

The coefficient of determination (R^2) of the relationship in Eq. (2) is 0.39, so the associated uncertainty appears to be significant. However, the negative relationship between AAE and MCE in Eq. (2) is robust as identified by previous studies (Saleh et al., 2014; Kirchstetter and Thatcher, 2012). For example, absorption of aerosols from biomass burning can be contributed by either BC or BrC, or both (Moise et al., 2015). As discussed above, the absorption of carbonaceous aerosols is mainly caused by BC at high MCE conditions (>0.9); in contrast, the BC/CA ratio is almost zero at low MCE conditions (<0.8) (McMeeking, 2008). Using Eq. (2), we calculate AAE values of 0.86 and 4.3 at MCE values of 1.0 and 0.8, respectively, and each calculated AAE is in good agreement with the observed BC (0.86) and BrC AAE (5.0) from biomass burning samples measured by Kirchstetter and Thatcher (2012).

161 Saleh et al. (2015) also showed that the BC to OC ratio (proportional to MCE) has negative
162 relationship with AAE.

163 In addition, we are able to obtain the BrC/BC absorption ratio using AAE. In
164 Appendix A, we present a detailed description of our method for estimating the relationship
165 between the BrC/BC absorption ratio and AAE. Figure 1 shows the estimated BrC/BC
166 absorption ratio at 550 nm as a function of MCE. Different lines indicate different AAEs of
167 BC and BrC according to the Table 1 of Kirchstetter and Thatcher (2012). They calculated
168 BC AAE and BrC AAE using 115 wood smoke samples. For the calculation of BrC AAE, BC
169 AAE had to be decided, and they assumed three different BC AAEs (0.86, 1.00, 1.15) based
170 on their smoke samples and previous studies. Resulting BrC AAEs were 5.00, 5.48, and 6.19.
171 We conduct three simulations according to the AAE values of Kirchstetter and Thatcher
172 (2012) (Figure 1), as described later in this section. For high MCE conditions (>0.95), the
173 BrC contribution to the CA absorption is negligible, whereas it becomes significant for low
174 MCE conditions (<0.85).

175 We calculate the MCE of biomass burning based on the Fire Inventory from NCAR
176 (FINN) (Wiedinmyer et al., 2011) with vegetation dependent emission factors of CO_2 and CO
177 using Eq. (3) as follows:

178 $$\mathrm{MCE} = \frac{\Delta C_{CO_2}}{\Delta C_{CO_2} + \Delta C_{CO}} = \frac{EF_{CO_2}/MW_{CO_2}}{EF_{CO_2}/MW_{CO_2} + EF_{CO}/MW_{CO}}, \quad (3)$$

179 where EF is the emission factor [g-species kg-dry matter^{-1}] and MW is the molecular weight
180 [g-species mole^{-1}].

181 Finally, mass absorption efficiency (MAE), which is used for converting light
182 absorption to mass concentration, is needed to obtain the BrC/BC mass ratio from the

183 BrC/BC absorption ratio. For the fresh BC MAE at 550 nm, we use the value of 7.5 $m^2 g^{-1}$
184 recommended by Bond and Bergstrom (2006) (Nakayama et al., 2013; Park et al., 2010). For
185 BrC, a large range of MAE values (0.09-4.1 $m^2 g^{-1}$ at 550 ± 30 nm) has been reported
186 (Alexander et al., 2008; Cheng et al., 2011; Chung et al., 2012; Clarke et al., 2007; Favez et
187 al., 2009; Hecobian et al., 2010; Hoffer et al., 2006; Kirchstetter et al., 2004; McMeeking,
188 2008; Yang et al., 2009). The highest MAE (3.6-4.1 $m^2 g^{-1}$ at 550 nm) was observed by
189 Alexander et al. (2008), who used transmission electron microscopy to identify the optical
190 properties of individual BrC particles in the atmosphere. Generally, low MAEs were reported
191 when analyzing water soluble organic carbon (WSOC) from water extracts (Cheng et al.,
192 2011; Hecobian et al., 2010; Srinivas and Sarin, 2014), indicating that WSOC may include
193 both BrC and colorless OC. Intermediate MAEs mostly came from optical measurements
194 (Chung et al., 2012; Favez et al., 2009; Yang et al., 2009). For the primary BrC MAE, we use
195 1.0 $m^2 g^{-1}$ at 550 nm based on McMeeking (2008), who conducted a number of MAE
196 measurements of biomass burning samples (~30 unique fuels tested in ~230 burns) using both
197 filter-based and optical-based methods. In brief, we use the MAE values of 7.5 $m^2 g^{-1}$ and 1.0
198 $m^2 g^{-1}$ at 550 nm for primary BC and BrC, respectively. But at a shorter wavelength, higher
199 MAE value was used for primary BrC (e.g., 5.3 $m^2 g^{-1}$ at 365 nm as discussed in Section 4).
200 Using the results in Figure 1 with Eq. (3), we calculate the EF (mass) ratio of BrC to
201 OC as summarized in Table 1. The EF ratio of BrC to OC differs for each vegetation type and
202 assumed BC AAE (0.86-1.15). Among different vegetation types, cropland burning shows the
203 highest BrC to OC mass ratio, driven by the low MCE and the highest ratio of BC to OC EF.
204 Because we calculate the BrC to OC EF ratio by multiplying the BrC to BC EF ratio by the
205 BC to OC ratio, the high BC to OC ratio can lead to a high BrC to OC ratio. Although Table 1

206 shows the highest BrC/OC ratio from cropland burning, its contribution to the global BrC
207 emission is small because the OC emission from the cropland is the lowest (Wiedinmyer et
208 al., 2011). Instead, the tropical forest burning is the highest, and the resulting total BrC
209 emission from biomass burning is 3.9 ± 1.7 TgC yr^{-1}, which contributes about $17 \pm 7\%$ of
210 total OC emission from biomass burning (22.7 TgC yr^{-1}) (Wiedinmyer et al., 2011).
211 Our method of estimating BrC emissions from biofuel use is similar to that of
212 estimating emissions from biomass burning. We estimate BrC/OC ratio using the MCE and
213 BC to OC ratio in the same way as the biomass burning estimates. The only difference is that
214 the biofuel emission of each sector is not known (the biomass burning emission is known for
215 each vegetation type). Therefore, we first estimate OC biofuel emissions from each biofuel
216 category with the information given by previous studies (Bond et al., 2007; Bond et al., 2004;
217 Fernandes et al., 2007). Because there is no clear evidence that BrC is emitted by dung,
218 charcoal, and the industrial sector, here we consider only fuelwood and agricultural residue as
219 BrC sources. Fuelwood burning is the largest contributor to biofuel BrC emission. Our
220 estimate of BrC/OC mass ratio is 0.271 - 0.663 from biofuel use. Overall results are
221 summarized in Table 2. Note that base year of Table 2 is 2000 because previous studies
222 reported their values based on 2000. We scale up the emission for 2007 as described in
223 Section 3.2. Resulting BrC emission from biofuel use is 3.0 ± 1.3 TgC yr^{-1}, which is
224 comparable to BrC emission from biomass burning.

225 **2.2 Secondary source**

226 We consider SOC as a source of BrC in the model based on the observed optical
227 characteristic of SOC, depending on its chemical formation, as follows: 1) anthropogenic
228 (aromatic) SOCs tend to absorb solar radiation more efficiently than biogenic SOCs

(Jacobson, 1999; Nakayama et al., 2010; Zhong and Jang, 2011; Zhong et al., 2012); 2) the solar absorption efficiency increases as SOCs undergo atmospheric aging processes (Bones et al., 2010; Lambe et al., 2013; Laskin et al., 2015; Laskin et al., 2010; Updyke et al., 2012); 3) SOCs formed in inorganic seeds have a darker color than others (Jaoui et al., 2008; Nakayama et al., 2013; Zhong and Jang, 2011; Zhong et al., 2012); moreover, SOCs become darker when they undergo aging in the presence of nitrogen-containing inorganic gases and aerosols (Bones et al., 2010; Laskin et al., 2010; Liu et al., 2012).

Among those factors, the first two are more important than the last. For example, the absorbance of aged biogenic SOCs produced in inorganic seeds is much lower than that of fresh anthropogenic SOCs under no-seed conditions (Zhong and Jang, 2011). Furthermore, Lambe et al. (2013) suggested that the effect of NOx on SOC light absorption is small under typical ranges of VOC/NOx. Therefore, here we consider the first two factors for BrC simulations in the model. We assume anthropogenic (aromatic) SOCs with high atmospheric aging as BrC in the model. Atmospheric aging is calculated using the volatility basis set (VBS) approach with six bins in the model (Jo et al., 2013), where SOC concentrations of the first two bins are considered as BrC. However, we note that some brown SOCs can be bleached when they undergo photodissociation (Zhong and Jang, 2011; Sareen et al., 2013). Furthermore, browning reactions can be accelerated by cloud and fog processing of aerosols (Moise et al., 2015), which are not considered in this study. More detailed treatments of the chemical aging of BrC are needed in future BrC models.

BrC from anthropogenic SOC has different optical properties (i.e, MAE, imaginary refractive index) compared with BrC from wood burning. Therefore, we apply different optical parameters for the model evaluation (Section 4) such as 5.3 m^2 g^{-1} (McMeeking,

252 2008) for primary BrC and 1.5 m^2 g^{-1} (Nakayama et al., 2010) for secondary BrC at 365 nm
253 (note that the MAE of primary BrC at 550 nm is 1.0 m^2 g^{-1} as discussed in Section 2.1). The
254 estimated annual amount of secondary BrC sources is 5.7 TgC yr^{-1}, which contributes 45% of
255 total BrC sources.
256
257 ## 3 Model description
258 ### 3.1 General
259 We use the GEOS-Chem (version 9.1.2) global 3-D chemical transport model (Bey et
260 al., 2001) to simulate BrC for 2007. The model is driven by Modern Era Retrospective-
261 analysis for Research and Applications (MERRA) assimilated meteorological data from the
262 Global Modeling and Assimilation Office Goddard Earth Observing System (Rienecker et al.,
263 2011). The data include winds, precipitation, temperature, boundary layer height, and other
264 meteorological variables at 0.5° × 0.667° horizontal resolutions, but are degraded to 2° × 2.5°
265 for computational efficiency.
266 We conduct a fully coupled oxidant-aerosol simulation, including SO_4^{2-} - NO_3^- -
267 NH_4^+, soil dust, and sea salt aerosols. The simulation of carbonaceous aerosols in the GEOS-
268 Chem is based on Park et al. (2003; 2006). The model carries BC and POC, with a
269 hydrophobic and hydrophilic fraction for each. We assume that 80% of BC and 50% of POC
270 are emitted as hydrophobic (the rest is hydrophilic), then hydrophobic aerosols become
271 hydrophilic with an e-folding time of 1.15 days (Cooke et al., 1999). For the SOC simulation,
272 we use the VBS approach based on Jo et al. (2013). All SOC is considered as hydrophilic,
273 and more details are described in previous SOC studies (Chung and Seinfeld, 2002; Henze
274 and Seinfeld, 2006; Henze et al., 2008; Jo et al., 2013; Liao et al., 2007). Note that we

consider only the carbon mass of OC including BrC as discussed below, to avoid uncertainties involved in converting organic carbon to organic matter concentrations, which is typically done by multiplying a constant ratio (e.g, 1.4-2.1) (Aiken et al., 2008; Turpin and Lim, 2001).

3.2 Emissions

We use fossil fuel and biofuel emissions of CAs for 2000 with no monthly variations from Bond et al. (2007). However, domestic wood burning for heating has strong seasonal dependency, so we additionally use the Monitoring Atmospheric Composition & Climate/City Zen (MACCity) emission inventory (Diehl et al., 2012; Granier et al., 2011) to obtain seasonal variations of global biofuel emissions and to scale up for 2007. For this, we divide the whole globe into regions with similar seasonality according to the Atmospheric Chemistry and Climate Model Intercomparison Project (ACCMIP) (Lamarque et al., 2010), which is the basis of the MACCity inventory. We apply the annual trend of each ACCMIP region to the emissions from Bond et al. (2007). The emissions for each region and trends are listed in Table S1 and Table S2.

We use biomass burning emissions from FINN version 1.0 (Wiedinmyer et al., 2011), which provides global daily estimates of trace gases and aerosols at 1 km horizontal resolution for 2002-2012 (http://bai.acd.ucar.edu/Data/fire/). However, the FINN version 1.0 inventory does not include aromatic VOCs (benzene, toluene, and xylene), the emissions of which are estimated by multiplying dry burned matter by emission factors from Akagi et al. (2011) and Andreae and Merlet (2001).

4 Model Evaluation

We conduct a model evaluation using the observed light absorption of WSOC

measured by Hecobian et al. (2010) and Zhang et al. (2011; 2013) in the United States. The model evaluation allows us not only to validate simulated BrC concentrations but also to examine each source contribution to BrC in the United States. We also use the global single scattering albedo (SSA) observations from the AERONET to evaluate the effect of including BrC on light absorption by aerosols over the globe.

4.1 United States

Prior to evaluating BrC simulations, we first focus on BC and OC aerosols in the model to examine the general model performance in simulating carbonaceous aerosol concentrations in the United States. We use BC and OC observations from the Interagency Monitoring of Protected Visual Environments (IMPROVE) network for 2007 (Malm et al., 1994). Most sites were situated in rural regions, measuring background concentrations of BC and OC. The data were available every three days; more than 20,000 samples were used for our comparison. For comparison with the model results, we computed the observed monthly mean concentrations of BC and OC averaged on the 2°×2.5° model grid.

Figure 2 shows scatterplot comparisons of the observed and simulated monthly mean BC and OC concentrations in the United States. The model slightly underestimates both BC and OC over the United States, consistent with similar comparisons in Huang et al. (2013). We calculate the annual mean concentrations of the model using the simulated values of model grid boxes corresponding to the IMPROVE network sites. The simulated annual mean BC concentration is 0.22 μgC m^{-3}, which is 12% lower than the observed mean value (0.25 μgC m^{-3}). However, the bias in the model is larger for OC by 30% (1.16 and 0.81 μgC m^{-3} for observed and simulated OC concentrations, respectively), which is additionally due to the underestimation of SOC in the model (Jo et al., 2013). This low bias for SOC can be reflected

321 in the simulated BrC concentrations, which is discussed later in this section.

322 We use the light absorption observations of WSOC measured using a UV-Vis
323 spectrophotometer and Long-Path absorption Cell by Hecobian et al. (2010), and compare
324 them with the light absorption by BrC in the model. Absorption coefficients of WSOC at 365
325 nm were measured at 15 sites in the southeastern United States in 2007. Among them, eight
326 sites are in urban areas, and the others are in rural regions. Detailed descriptions of the
327 measurements are available in Hecobian et al. (2010).

328 Because light absorption observations are measured only for water soluble fractions
329 of OC, and do not include water insoluble components, we separate BrC in the model into
330 water soluble and water insoluble components. The model divides OC (or BrC) into
331 hydrophilic and hydrophobic components. For the comparison, we do not use the simulated
332 hydrophilic fraction, but instead use an observed WSOC/OC ratio because the assumed
333 division of hydrophobic and hydrophilic fractions of OC and their conversion can be
334 applicable in a global sense, but in a regional sense, it may cause a significant discrepancy.
335 For example, the observed water soluble fraction of the total OC is generally low (on the
336 order of 25%) in the Los Angeles basin (Zhang et al., 2013), on the other hand, the model
337 simulates a high water-soluble fraction of the total OC (63-74%) in this region. For this
338 reason, we decide to use the observed WSOC/OC ratio for the evaluations. In the
339 southeastern United States, the observed WSOC/OC ratio is about 0.58 (Weber et al., 2007;
340 Zhang et al., 2013), which is also used to estimate the water soluble BrC concentrations from
341 the total BrC concentrations in the model.

342 Because the model simulates a mass concentration of BrC, a conversion from the
343 mass concentration to light absorption is carried out by multiplying MAE values. For BrC

344 from wood burning, we use the MAE value of 5.3 m^2 g^{-1} at 365 nm measured by McMeeking
345 (2008) in order to retain the consistency between our emission estimates and the evaluation.
346 For BrC from SOC, we select the MAE of 1.5 m^2 g^{-1} at 365 nm calculated by Nakayama et al.
347 (2010) (see Figure 4 in their paper).
348 Figure 3 shows monthly mean simulated and observed light absorption coefficients of
349 BrC at 365 nm averaged over all sites in the southeastern United States for 2007. Black
350 circles and colored bars indicate the observed and simulated BrC absorption at 365 nm,
351 respectively, and different colors in the bar show contributions from different sources. Each
352 panel represents different model simulations with each case for AAE selections as shown in
353 Figure 1 and Table 1.
354 In winter months (November through March), the observed light absorptions were
355 generally high and reached a peak in March. These high absorptions were highly correlated
356 with levoglucosan, which is a marker for biomass burning (Hecobian et al., 2010). During the
357 summer, the observed light absorptions decreased substantially.
358 The model generally captures the observed seasonal variation with high absorption in
359 the winter, having a peak in March and low absorption in the summer (R of 0.93). On an
360 annual mean basis, we find that the model is too high by 46% for case 1, and is too low by -
361 31% for case 3, relative to the observations, respectively. The model for case 2 is in the best
362 agreement with the observations (4%) on an annual mean basis.
363 The BrC source contribution in the model is similar to the observed source
364 contribution. Hecobian et al. (2010) showed that biomass burning was the main contributor
365 for the winter season, whereas the SOC contribution increased during the summer season.
366 The simulated seasonal variation is consistent with the observation, as shown in Figure 3. The

annual mass contribution of SOC to BrC is 38% (in case 2), which is in good agreement with the observed contribution of 32% (Hecobian et al., 2010). Based on the results in Figure 3, the model for the case 2 yields best estimates of BrC emissions.

In addition to the observation by Hecobian et al. (2010), we use the light absorption observations by Zhang et al. (2011; 2013). Measurements were carried out in Atlanta, GA (33.778427N, 84.396181W), Pasadena, CA (34.140528N, 118.122455W), and Riverside, CA (33.97185N, 117.32266W) for a month or less. As discussed above, we apply the observed WSOC/OC ratio to the model BrC concentrations: 26% for the Los Angeles basin (Pasadena and Riverside) (Zhang et al., 2013) and 58% for Atlanta (Weber et al., 2007; Zhang et al., 2013).

Figure 4 shows the daily mean observed and simulated light absorption coefficients from the best model (case 2) for Atlanta, Pasadena, and Riverside for 2010. The upper panel shows the comparison of the observed versus simulated light absorption for Atlanta. The highest observed daily absorption occurred on August 24, but the model fails to reproduce it. Furthermore, the model generally overestimates the observed absorption by 44%, and the large discrepancies mainly occur in September. This large discrepancy in September is similar to the result shown in Figure 3(b) for 2007.

The middle and lower panels show the comparisons at the Los Angeles basin sites in May and June. The observed mean light absorptions at these sites (0.81 and 0.98 Mm^{-1} for Pasadena and Riverside, respectively) are higher than the observed mean light absorption (0.56 Mm^{-1}) for Atlanta. However, the model underestimates the observations by 38% (Pasadena) and 48% (Riverside). Zhang et al. (2013) showed that the main sources of BrC at these sites were SOC from anthropogenic emissions. The model also shows a high

390 contribution (85%) of the secondary source to the total BrC mass concentrations, but the
391 magnitudes are generally lower than the observations, and this low bias is likely related to
392 underestimation of the simulated SOC concentrations using the 1-D VBS (Jo et al., 2013).
393 We find from the model evaluation over the United States that the model generally
394 captures the observed mean absorption and its seasonal variability in the region where
395 primary sources are dominant. On the other hand, the model underestimates the observed
396 mean absorption in the region with the dominant secondary sources. The low bias is partly
397 explained by the SOC underestimation in the model. However, the underestimations of BrC
398 from SOC (38-48%) are higher than those of SOC (18%), indicating the importance of
399 additional secondary BrC sources that we did not include in the model.
400 A MAE value for secondary BrC could be another possible reason for the bias in the
401 model. Although chamber studies suggested weak absorbing characteristics of BrC from SOC
402 (Nakayama et al., 2010; Nakayama et al., 2013; Zhong and Jang, 2011), some field
403 observations speculated the existence of strongly-absorbing BrC from SOC (Alexander et al.,
404 2008; Chung et al., 2012). For example, applying the MAE value of 3.5 m^2 g^{-1} at 365 nm (a
405 half of the MAE at 365 nm from Alexander et al. (2008)) for secondary BrC yields a similar
406 mean absorption value to the observation over LA basin. Extensive observations of optical
407 characteristics of BrC depending on the formation mechanisms would be needed to reduce
408 the associated uncertainties and to improve the model.

409 **4.2 Evaluation against global AERONET observations**

410 No global observation of BrC is available yet. Here we use the observed SSA at
411 AERONET sites to evaluate the model by focusing on the effect of BrC on the simulated
412 aerosol absorption. We also use observed aerosol optical depth (AOD) to evaluate the model

capability to simulate aerosol mass concentrations.

For comparisons of AOD and SSA between the model and observations, we use FlexAOD (http://pumpkin.aquila.infn.it/flexaod/), which calculates AOD and SSA using simulated aerosol mass concentrations from GEOS-Chem with the Mie algorithm (Mischenko et al., 2002; Curci et al., 2015).

For optical properties of BrC, we use imaginary refractive indices of BrC from McMeeking (2008) for wood burning sources, and from Nakayama et al. (2010) for SOC sources. Detailed description of the values used in AOD and SSA calculation are provided in Section 6, where we discuss the DRE of BrC.

Figure 5 shows comparisons of monthly mean simulated versus observed AOD at 500 nm, SSA at 440 nm. We find that the model captures the observed AOD quite well with a regression slope of 0.86 and a R of 0.88. However, the model tends to overestimate the observed SSA, implying that the simulated aerosol concentrations appear to have too large a fraction of scattering aerosols. We find that the inclusion of BrC in the model reduces the high bias of simulated SSA by 33% and 23% (lower left and lower right panel of Figure 5), indicating a considerable contribution of BrC to aerosol absorption. Although the statistics suggest a greater improvement with the case 1 in terms of the bias, simulated SSA values at sites in Africa with high BrC concentrations, are too low apart from the regression line (discrepancy > 0.1). This result also supports our selection of the case 2 as the best model for BrC emission estimates.

Despite a decrease of simulated SSA with BrC, the model is still too high relative to the observations. The overestimation might be partly caused by the underestimation of BC emissions from biomass burning (Bond et al., 2013). This is also supported by the fact that

436 the discrepancy gets larger for biomass burning regions, where a difference between the
437 model and AERONET SSA is 40% higher than that in regions with high anthropogenic
438 emissions. Emission factors of BC used in this study are 0.2-0.69 g kg^{-1} (Wiedinmyer et al.,
439 2011), which are lower than the value of 1 g kg^{-1} used by Chin et al. (2009), who found no
440 significant bias in their model compared with the AERONET SSA. Lin et al. (2014) also
441 reported a small bias in their model compared with AERONET SSA using 4.7 Tg yr^{-1} of
442 global annual biomass burning BC emissions, which is about two times higher than 2.2 Tg yr^{-1}
443 of this study.

444 In addition to the biomass burning emission of BC, the anthropogenic emission of BC
445 could also contribute to the simulated SSA bias. Cohen and Wang (2014) showed that a
446 global top-down emission of BC is twice as large as the bottom-up estimates of BC based on
447 the Kalman Filter approach. They suggested that BC emissions in East Asia, Southeast Asia,
448 and Eastern Europe are significantly underestimated in current bottom-up emission
449 inventories. This issue is critically important, and possibly has an important implication for
450 climate. However, an investigation of BC emissions for the SSA discrepancy above is beyond
451 the scope of our work, and will be conducted in future studies.

452 Light absorption enhancement of aged BC could also be one of the reasons for the
453 SSA overestimation in the model. Here we use the same optical parameters for all BC in the
454 model. However, Bond et al. (2006) suggested that the absorption of aged BC is about 1.5
455 times greater than that of fresh BC. BC aging occurs as it is mixed internally with other
456 aerosols. If we assume hydrophilic BC as aged BC in the model and its absorption
457 enhancement by a factor of 1.5 relative to hydrophobic BC, the high bias of simulated SSA is
458 additionally reduced by about 20% (not shown). Considering all these uncertainties, however,

459 our evaluation above indicates that the model for the case 2 results in the best estimates of
460 simulated BrC concentrations, which will be used for examining BrC effects on climate and
461 photochemistry, below and other two cases are considered as upper and lower limits of our
462 estimates.
463
464 ## 5 Global budgets
465 ### 5.1 Annual surface concentration
466 Figure 6 shows our best estimates of annual mean concentrations of BrC and each
467 source contribution in surface air for 2007. Values are high in regions where biomass burning
468 (Southeast Asia and South America) and biofuel (East Asia and Northeast India) sources are
469 dominant. These primary sources account for 77% of BrC concentrations in surface air. On
470 the other hand, secondary sources are relatively minor in the surface, but their contribution
471 increases in the free troposphere, as discussed in Section 5.2.
472 Figure 7 shows BrC to BC and OC ratios in surface air in the model. The BrC to BC
473 ratio is highest over the eastern North Pacific and the North Atlantic. This high ratio over the
474 ocean reflects a secondary chemical production, which contributes to BrC but not to BC.
475 Over the continents, the ratio is generally higher in heavy biomass burning regions (South
476 America and Africa) than in industrialized regions (East Asia, Europe, and the eastern United
477 States) because more BrC than BC is emitted from biomass burning.
478 Similarly, the BrC to OC ratio is also high over the oceans because of secondary BrC,
479 the concentrations of which increase with atmospheric aging. Over the continents, the ratio is
480 smaller reflecting relatively fresh emissions of OC from anthropogenic sources that do not
481 directly contribute to BrC. We find that the BrC to OC ratio is relatively high in regions with

large biofuel use (North India and Central Asia). Although China is one of the largest emission source regions for BrC (Figure 6), both BrC to BC and BrC to OC ratios are relatively low because of high concentrations of BC and OC. Our global mean BrC to BC and BrC to OC ratios at the surface are 1.24 and 0.21, respectively and are lower than the ratio (3.4 of BrC to BC ratio and 0.43 of BrC to OC ratio in terms of burden) of Feng et al. (2013), but higher than the ratio (1.0 of BrC to BC ratio) used in Park et al. (2010).

5.2 Tropospheric budget of BrC

Table 3 summarizes our best estimates of the global tropospheric budgets of BrC, along with BC and OC. The global BrC source is 12.5 ± 3.0 TgC yr^{-1}, which accounts for 27% of OC sources. Although the biofuel emission (6.5 TgC yr^{-1}) is three times lower than the biomass burning emission (22.7 TgC yr^{-1}) for OC, the biofuel emission (3.0 ± 1.3 TgC yr^{-1}) becomes significant for BrC, contributing about 43% of primary sources. The secondary source of BrC is 5.7 TgC yr^{-1}, and is comparable to the primary sources (6.8 ± 3.0 TgC yr^{-1}).

Wet deposition is the main removal process for BrC, and accounts for 86 % of total removal processes. The remaining loss is due to dry deposition. The contribution of wet deposition to total deposition of BrC is similar to that of OC (82%), because we treat BrC scavenging similarly to that of OC. Because secondary BrC is produced all over the troposphere (not only at the surface) and is hydrophilic, most secondary BrC is removed by wet deposition processes (92%).

The global burden of BrC shows the highest contribution from secondary BrC (50 %) compared to primary contributions from biomass burning (30 %) and biofuel (20 %). This result is opposite to the source contributions in surface air shown in Figure 6. The contribution of secondary BrC to the atmospheric burden is twice as high as the contribution

of secondary BrC to the surface concentration (23%), reflecting a relatively large production of BrC in the free troposphere as well as limited export of primary BrC from the surface to the free troposphere.

Our BrC lifetime is 5.8 days, which is lower than that of OC (7.9 days) because of different contributions of the secondary sources for BrC and OC. The latter species includes a larger fraction of secondary species (52%), the lifetime of which is usually longer than that of POC especially for not aged biogenic SOC (Jo et al., 2013). No significant difference between the lifetimes of BrC and BC exists because BrC, which is more hydrophilic than BC, is more prone to wet scavenging than BC.

6 Direct radiative effect of BrC

We use imaginary refractive indices of BrC as a function of wavelength for radiative transfer calculations to account for the wavelength dependency of the BrC absorption. Imaginary refractive indices in the literature have a wide range of values, even from the same sources, such as wood burning (Chakrabarty et al., 2010; Kirchstetter et al., 2004; McMeeking, 2008). In order to maintain the consistency with BrC emission estimates from primary sources, we use the imaginary refractive indices reported by McMeeking (2008), which are 0.18, 0.14, and 0.10 at 370, 405, and 532 nm, respectively. The values are interpolated with the AAE at every 50 nm wavelength interval for the radiative transfer calculations. For secondary BrC, values from Nakayama et al. (2010) are used with 0.047 and 0.007 at 355 and 532 nm, respectively, based on the measurements for SOC from toluene.

We calculate AOD, SSA, and asymmetry parameter using FlexAOD, which is described in Section 4.2. Note that we calculate DRE rather than DRF. DRE is the

528 instantaneous radiative impact of all atmospheric particles on the Earth's energy balance, and
529 DRF is the change in DRE from pre-industrial to present-day (Heald et al., 2014). We use the
530 Rapid Radiative Transfer Model for GCMs (RRTMG) (Iacono et al., 2008) for DRE
531 calculations. Wavelengths used for the calculation are 300, 304, 393, 533, 702, 1010, 1270,
532 1462, 1784, 2046, 2325, 2788, 3462, and 8021 nm. MERRA reanalysis data are used for
533 albedo and other meteorological variables.

534 Figures 8(a) and 8(b) show the clear sky DRE values of primary and secondary BrC
535 concentrations. Because the imaginary refractive indices of BrC are between those of
536 strongly absorbing BC and scattering OC, the global mean DRE of BrC is close to zero, as
537 shown in (a) and (b).

538 Although the DRE of BrC at the top of the atmosphere is nearly zero, the increased
539 DRE of OC after considering BrC absorption (usually considered as scattering OC) is 0.11 W
540 m^{-2}, as shown in Figure 8(c). The DRE of OC without BrC absorption is -0.69 W m^{-2} (Figure
541 8(d)), and this value is increased to -0.58 W m^{-2} after considering BrC absorption.
542 Consequently, the cooling effect of OC is reduced by 16%.

543 Despite the negligible effect of BrC on DRE or DRF, its significance manifests for
544 OC DRF estimates, which have been conducted based on the assumption of scattering OC.
545 For example, AeroCom phase II simulations calculated -0.03 W m^{-2} as the global mean DRF
546 of POC from fossil fuel and biofuel, and -0.06 W m^{-2} for that of SOC (Myhre et al., 2013).
547 Because the biofuel emission is about twice as large as the fossil fuel emission (Bond et al.,
548 2007), and one-half of OC from biofuel is BrC, one-third of the POC from fossil fuel and
549 biofuel is BrC. Therefore, one-third of DRF (-0.01 W m^{-2}) of POC in AeroCom is related to
550 BrC, whose DRF is close to zero. For SOC, because the pre-industrial biogenic SOC

concentration is similar to present-day conditions, almost all DRF of SOC is from anthropogenic SOC. Based on previous SOC studies (Henze et al., 2008; Jo et al., 2013; Murphy and Pandis, 2010), approximately one-third of anthropogenic SOC is highly aged, and can thus be assumed to be BrC in this simple estimation. As a result, one-third of DRF (-0.02 W m^{-2}) of SOC in AeroCom is related to BrC. The total DRF of BrC that was assumed to be scattering OC in the AeroCom study is -0.03 W m^{-2}. Because DRF of BrC is almost negligible, the negative DRF of OC (-0.09 W m^{-2}) in AeroCom could likely be overestimated by 50%. We think, however, the warming effect of BrC on the negative DRF or DRE of OC would be a low-end value because our best model likely underestimates BrC concentrations especially from the secondary source.

7 Effect on ozone photochemistry

BrC absorption, particularly at UV wavelengths, has an important implication for ozone photochemistry. Here we examine the effect of BrC absorption on photochemistry by updating photolysis rate calculations in GEOS-Chem following Martin et al. (2003). Table 4 shows the calculated extinction efficiency and SSA of important aerosols at 0.4 μm, which affect UV extinction, and thus photolysis rate calculations, in the model. Values of OC, BC, and inorganic aerosols are from GEOS-Chem, in which we update aerosol optical properties by adding those of BrC. We include optical properties of primary and secondary BrC separately because they differ substantially. For example, SSA values of primary BrC are smaller than those of secondary BrC, and thus have a greater impact on UV radiation. Compared with other aerosols, SSA values of BrC are generally lower than those of OC and inorganic aerosols, but higher than those of BC.

574 Martin et al. (2003) showed that the effects of aerosols on photolysis rates increased
575 CO by 5-15 ppbv in the remote Northern Hemisphere (annual mean concentrations less than
576 140 ppbv). This increase resulted in an improved model agreement with observations, but
577 there was a still gap between the model and the observations. In our simulation with BrC, CO
578 concentration is further increased by 0.2-1.9 ppbv in remote Northern Hemisphere regions
579 (annual mean concentrations less than 140 ppbv in the model). On the other hand, OH
580 concentrations are decreased by 0-10% in the boundary layer over the Northern Hemisphere
581 (maximum decreases occur in regions with high BrC concentrations, shown in Figure 6). The
582 change of OH owing to BrC is about one-third of the OH change according to the overall
583 aerosol effects from Martin et al. (2003). Therefore, the inclusion of BrC significantly affects
584 tropospheric chemistry, especially for regions with heavy biomass burning and biofuel
585 emissions.
586 Finally, we quantify the effects of BrC on global NO_2 photolysis rates and ozone
587 concentrations at the surface. Figure 9 shows changes in annual NO_2 photolysis rates and O_3
588 concentrations in surface air owing to BrC absorption. Although BrC absorption is included,
589 there are no significant changes (less than 1%) of the global mean NO_2 photolysis rate and O_3
590 concentration in surface air. However, the effect of BrC appears to be important for regions
591 with high BrC concentrations. We find a maximum decrease of the annual mean NO_2
592 photolysis rate by 8% in surface air over Asia where the resulting reduction of O_3
593 concentration is up to -2 ppbv (6% of annual mean surface O_3 concentration). We also find
594 that the BrC effect has a strong seasonal variation such that it is maximized in the spring
595 when surface O_3 concentration is decreased up to -13% in Asia because of high BrC
596 concentration (55 $\mu gC\ m^{-3}$). This maximum O_3 decrease by BrC (-13%) is similar to the O_3

decrease (15%) by fire aerosols in Jiang et al. (2012).

8 Conclusion

OC has been considered to be a scattering aerosol, but emerging evidence has shown that some OC can efficiently absorb solar radiation. This absorbing OC is called BrC. With increasing recognition of its importance, especially for solar absorption at UV and short visible wavelengths, quantification of its spatial and temporal distribution is much needed for the study of climate and air quality issues. Here we conducted an explicit global BrC simulation for the full year of 2007 using a global 3-D chemical transport model (GEOS-Chem), and examined its implication for climate and O_3 photochemistry.

We first estimated primary BrC emissions from biomass burning and biofuel use based on the relationship between AAE and MCE. Our estimates of primary BrC emissions are 3.9 ± 1.7 and 3.0 ± 1.3 TgC yr^{-1} from biomass burning and biofuel use, respectively. The secondary BrC source is estimated to be 5.7 TgC yr^{-1} from the aromatic oxidation.

With explicit BrC emissions, a coupled oxidant-aerosol simulation was conducted for 2007 to obtain the spatial and temporal distributions of BrC concentrations. We first evaluated the model by comparing the simulated versus observed BrC absorption in the United States and found that the model successfully reproduced the observed seasonal variation in the southeastern United States, whereas the model significantly underestimated secondary BrC over the Los Angeles basin.

Our budget analysis showed that BrC from primary sources are dominant (77%) in surface air, but BrC from secondary sources becomes important with increasing altitudes. For example, BrC from secondary sources accounts for the 50% of the tropospheric BrC burden,

620 which is higher than its 23% contribution to surface BrC concentrations. Our global mean
621 value of the BrC to BC ratio is 1.83 for the whole atmosphere, and 1.24 for the surface, which
622 significantly differs from the values used in previous studies.
623 Using our best results, we estimated the DRE of BrC to be close to zero at the top of
624 the atmosphere because the imaginary refractive indices of BrC are in the midpoint between
625 those of BC and OC. Despite a negligible contribution to DRE, the inclusion of BrC
626 absorption in the model offsets the negative radiative effect of OC by 0.11 W m^{-2} (16%).
627 Finally, we included BrC absorption in photolysis rate calculations in the model. We
628 found that the NO_2 photolysis rate is decreased up to 8%, especially for Asia, where BrC
629 concentration is high. Resulting annual surface O_3 concentrations are decreased up to -2 ppbv
630 (6%). This effect is more important in the spring, when a typical O_3 maximum occurs in Asia,
631 where the effect of BrC decreases the surface O_3 concentration by up to -13%.
632 Many chemical transport models and air quality models have included the effect of
633 aerosols on photolysis rate calculations, but have not considered the BrC effect. Based on our
634 analysis, BrC absorption could have a significant direct impact on regional air quality by
635 being involved in O_3 photochemical formation. Its significance, however, can be expanded to
636 the globe by its effect on the atmospheric oxidation capacity, which has an indirect but
637 important implication for global air quality and climate.
638
639 **Appendix A**
640 **A1 Relationship between BrC/BC absorption ratio and AAE**
641 In this section we describe a procedure for obtaining the relationship between the
642 BrC/BC absorption ratio and AAE. Assuming no internal mixing and dust influence, total

absorption at a certain wavelength (λ) can be expressed as:

$$\alpha_{\lambda,CA} = \alpha_{\lambda,BrC} + \alpha_{\lambda,BC} \quad \text{(A1)}$$

Rewriting Eq. (A1) using AAE:

$$\alpha_{\lambda_0,CA}\left(\frac{\lambda}{\lambda_0}\right)^{-A_{CA}^{O}} = \alpha_{\lambda_0,BrC}\left(\frac{\lambda}{\lambda_0}\right)^{-A_{BrC}^{O}} + \alpha_{\lambda_0,BC}\left(\frac{\lambda}{\lambda_0}\right)^{-A_{BC}^{O}} \quad \text{(A2)}$$

Dividing each side of Eq. (A2) by $\alpha_{\lambda_0,BC}$:

$$(1+F)\left(\frac{\lambda}{\lambda_0}\right)^{-A_{CA}^{O}} = F\left(\frac{\lambda}{\lambda_0}\right)^{-A_{BrC}^{O}} + \left(\frac{\lambda}{\lambda_0}\right)^{-A_{BC}^{O}} \quad \text{(A3)}$$

where F is the BrC/BC absorption ratio at λ_0.

We can solve Eq. (A3) analytically, and the procedure is described in Appendix A2. We do not use the analytical relationship because it uses only three wavelengths for the calculations. The Ångström relationship is based on empirical fitting. AAE varies in different wavelength regions, even if we use the same samples. For example, Chung et al. (2012) showed that CA AAE is about 1.2 when the first four wavelengths (370, 470, 520, 590 nm) are used, while the CA AAE is 1.35 with the last four wavelengths (590, 660, 880, 950 nm). This discrepancy is much increased in the case of BrC AAE. Liu et al. (2014) showed that BrC AAE varies by approximately 20%, depending on wavelength pairs. Furthermore, if we calculate AAE of BrC using the mass absorption efficiency (MAE) of Kirchstetter et al. (2004), AAE of BrC in all wavelengths (from 350 to 650 nm, 7 values) is fitted to 5.9 with a R^2 of 0.96. However, the AAE of BrC using just two wavelengths is 4.1 for the 350-440 nm and 8.0 for the 550-600 nm, respectively.

Therefore, we calculate the relationship between MCE and F by regression using multiple wavelengths: [300, 350, 400, 450, 500, 550, 600, 650, 700, 750, 800, 850, 900 nm].

If we rewrite Eq. (A3) for the regression form,

$$\overset{\circ}{A}_{CA}\,\log(\lambda) + C = -\log\left[F\left(\frac{\lambda}{\lambda_0}\right)^{-\overset{\circ}{A}_{BrC}} + \left(\frac{\lambda}{\lambda_0}\right)^{-\overset{\circ}{A}_{BC}}\right] \quad \text{(A4)}$$

where the residual term C is

$$C = -\overset{\circ}{A}_{CA}\,\log(\lambda_0) - \log(1+F) \quad \text{(A5)}$$

The left side of Eq. (A4) has the shape of Ax+B. Therefore, by linear regression analysis, we can obtain $Å_{CA}$ (the slope of the regression) as varying F on the right side. We choose an $Å_{BrC}$ values of {5.0, 5.48, 6.19} and an $Å_{BC}$ values of {0.86, 1.00, 1.15}, following Kirchstetter and Thatcher (2012), who estimated mean $Å_{BrC}$ using several wood samples (87 samples) over the 360 to 700 nm spectrum range. We assign a λ_0 value of 550 nm. The coefficient of determination (R^2) is greater than 0.98 in all the regression analyses. The calculated relationship between MCE and F is plotted in Figure 1. As expected, emissions of BrC are increased when MCE is decreased.

A2 Analytical derivation of Eq. (A3)

Here we describe the procedure to obtain the analytical relationship between MCE and F. First, substituting λ_1 and λ_2 in Eq. (A3),

$$(1+F)\left(\frac{\lambda_1}{\lambda_0}\right)^{-\overset{\circ}{A}_{CA}} = F\left(\frac{\lambda_1}{\lambda_0}\right)^{-\overset{\circ}{A}_{BrC}} + \left(\frac{\lambda_1}{\lambda_0}\right)^{-\overset{\circ}{A}_{BC}} \quad \text{(A6)}$$

$$(1+F)\left(\frac{\lambda_2}{\lambda_0}\right)^{-\overset{\circ}{A}_{CA}} = F\left(\frac{\lambda_2}{\lambda_0}\right)^{-\overset{\circ}{A}_{BrC}} + \left(\frac{\lambda_2}{\lambda_0}\right)^{-\overset{\circ}{A}_{BC}} \quad \text{(A7)}$$

Assuming AAE between λ_0 and λ_1 is equal to AAE between λ_0 and λ_2, divide Eq. (A6) by Eq.

683 (A7), and rearrange terms:

684 $$\left(\frac{\lambda_1}{\lambda_2}\right)^{-\mathring{A}_{CA}} = \frac{F\left(\frac{\lambda_1}{\lambda_0}\right)^{-\mathring{A}_{BrC}} + \left(\frac{\lambda_1}{\lambda_0}\right)^{-\mathring{A}_{BC}}}{F\left(\frac{\lambda_2}{\lambda_0}\right)^{-\mathring{A}_{BrC}} + \left(\frac{\lambda_2}{\lambda_0}\right)^{-\mathring{A}_{BC}}} \quad \text{(A8)}$$

685 Taking the logarithm of both sides:

686 $$\mathring{A}_{CA} = -\log\left(\frac{F\left(\frac{\lambda_1}{\lambda_0}\right)^{-\mathring{A}_{BrC}} + \left(\frac{\lambda_1}{\lambda_0}\right)^{-\mathring{A}_{BC}}}{F\left(\frac{\lambda_2}{\lambda_0}\right)^{-\mathring{A}_{BrC}} + \left(\frac{\lambda_2}{\lambda_0}\right)^{-\mathring{A}_{BC}}}\right) / \log\left(\frac{\lambda_1}{\lambda_2}\right) \quad \text{(A9)}$$

687 Substituting Eq. (2) into Eq. (A9) gives:

688 $$\mathrm{MCE} = \left[18.2 + \log\left(\frac{F\left(\frac{\lambda_1}{\lambda_0}\right)^{-\mathring{A}_{BrC}} + \left(\frac{\lambda_1}{\lambda_0}\right)^{-\mathring{A}_{BC}}}{F\left(\frac{\lambda_2}{\lambda_0}\right)^{-\mathring{A}_{BrC}} + \left(\frac{\lambda_2}{\lambda_0}\right)^{-\mathring{A}_{BC}}}\right) / \log\left(\frac{\lambda_1}{\lambda_2}\right)\right] / 17.34 \quad \text{(A10)}$$

689 After assigning $\mathring{A}_{BrC}$, $\mathring{A}_{BC}$, and the corresponding three wavelengths (λ_0, λ_1 and λ_2) in Eq.

690 (A10), we obtain the relationship between MCE and F analytically.

691

692 **Acknowledgements**

693 This study was supported by the Eco Innovation Program of KEITI (ARQ201204015) and by

694 Korea Ministry of Environment as "Climate Change Correspondence Program".

695

696

697

References

Aiken, A. C., DeCarlo, P. F., Kroll, J. H., Worsnop, D. R., Huffman, J. A., Docherty, K. S., Ulbrich, I. M., Mohr, C., Kimmel, J. R., and Sueper, D.: O/C and OM/OC ratios of primary, secondary, and ambient organic aerosols with high-resolution time-of-flight aerosol mass spectrometry, Environmental Science & Technology, 42, 4478-4485, 2008.

Akagi, S., Yokelson, R., Wiedinmyer, C., Alvarado, M., Reid, J., Karl, T., Crounse, J., and Wennberg, P.: Emission factors for open and domestic biomass burning for use in atmospheric models, Atmospheric Chemistry and Physics, 11, 4039-4072, 2011.

Alexander, D. T. L., Crozier, P. A., and Anderson, J. R.: Brown carbon spheres in East Asian outflow and their optical properties, Science, 321, 833, 2008.

Andreae, M. and Gelencser, A.: Black carbon or brown carbon? The nature of light-absorbing carbonaceous aerosols, Atmospheric Chemistry and Physics, 6, 3131-3148, 2006.

Andreae, M. O. and Merlet, P.: Emission of trace gases and aerosols from biomass burning, Global Biogeochemical Cycles, 15, 955-966, 2001.

Bahadur, R., Praveen, P. S., Xu, Y., and Ramanathan, V.: Solar absorption by elemental and brown carbon determined from spectral observations, Proceedings of the National Academy of Sciences, 109, 17366-17371, 2012.

Bey, I., Jacob, D. J., Yantosca, R. M., and Logan, J. A.: Global modeling of tropospheric chemistry with assimilated meteorology- Model description and evaluation, Journal of Geophysical Research, 106, 073-023,095, 2001.

Bond, T. C. and Bergstrom, R. W.: Light absorption by carbonaceous particles: An investigative review, Aerosol Science and Technology, 40, 27-67, 2006.

Bond, T. C., Bhardwaj, E., Dong, R., Jogani, R., Jung, S., Roden, C., Streets, D. G., and Trautmann, N. M.: Historical emissions of black and organic carbon aerosol from energy-related combustion, 1850-2000, Global Biogeochemical Cycles, 21, 2007.

Bond, T. C., Doherty, S. J., Fahey, D. W., Forster, P. M., Berntsen, T., DeAngelo, B. J., Flanner, M. G., Ghan, S., Kärcher, B., Koch, D., Kinne, S., Kondo, Y., Quinn, P. K., Sarofim,

726 M. C., Schultz, M. G., Schulz, M., Venkataraman, C., Zhang, H., Zhang, S., Bellouin, N.,
727 Guttikunda, S. K., Hopke, P. K., Jacobson, M. Z., Kaiser, J. W., Klimont, Z., Lohmann, U.,
728 Schwarz, J. P., Shindell, D., Storelvmo, T., Warren, S. G., and Zender, C. S.: Bounding the
729 role of black carbon in the climate system: A scientific assessment, Journal of Geophysical
730 Research, doi: 10.1002/jgrd.50171, 2013. n/a-n/a, 2013.

731 Bond, T. C., Habib, G., and Bergstrom, R. W.: Limitations in the enhancement of visible light
732 absorption due to mixing state, Journal of Geophysical Research: Atmospheres (1984–2012),
733 111, 2006.

734 Bond, T. C., Streets, D. G., Yarber, K. F., Nelson, S. M., Woo, J. H., and Klimont, Z.: A
735 technology-based global inventory of black and organic carbon emissions from combustion,
736 Journal of Geophysical Research, 109, 14203, 2004.

737 Bones, D. L., Henricksen, D. K., Mang, S. A., Gonsior, M., Bateman, A. P., Nguyen, T. B.,
738 Cooper, W. J., and Nizkorodov, S. A.: Appearance of strong absorbers and fluorophores in
739 limonene-O3 secondary organic aerosol due to NH4+-mediated chemical aging over long
740 time scales, Journal of Geophysical Research, 115, D05203, 2010.

741 Chakrabarty, R., Moosmüller, H., Chen, L. W. A., Lewis, K., Arnott, W., Mazzoleni, C.,
742 Dubey, M., Wold, C., Hao, W., and Kreidenweis, S.: Brown carbon in tar balls from
743 smoldering biomass combustion, Atmospheric Chemistry and Physics, 10, 6363-6370, 2010.

744 Chakrabarty, R. K., Pervez, S., Chow, J. C., Watson, J. G., Dewangan, S., Robles, J., and
745 Tian, G.: Funeral pyres in South Asia: Brown carbon aerosol emissions and climate impacts,
746 Environmental Science & Technology Letters, 1, 44-48, 2014.

747 Cheng, Y., He, K. B., Zheng, M., Duan, F. K., Du, Z. Y., Ma, Y. L., Tan, J. H., Yang, F. M.,
748 Liu, J. M., and Zhang, X. L.: Mass absorption efficiency of elemental carbon and water-
749 soluble organic carbon in Beijing, China, Atmospheric Chemistry and Physics, 11, 11497-
750 11510, 2011.

751 Chin, M., Diehl, T., Dubovik, O., Eck, T., Holben, B., Sinyuk, A., and Streets, D.: Light
752 absorption by pollution, dust, and biomass burning aerosols: a global model study and
753 evaluation with AERONET measurements, Annales Geophysicae, 27, 3439-3464, 2009.

754 Chung, C., Kim, S. W., Lee, M., Yoon, S. C., and Lee, S.: Carbonaceous aerosol AAE

755 inferred from in-situ aerosol measurements at the Gosan ABC super site, and the implications
756 for brown carbon aerosol, Atmospheric Chemistry and Physics, 12, 6173-6184, 2012.

757 Chung, S. and Seinfeld, J.: Global distribution and climate forcing of carbonaceous aerosols,
758 Journal of Geophysical Research, 107, 4407, 2002.

759 Clarke, A., McNaughton, C., Kapustin, V., Shinozuka, Y., Howell, S., Dibb, J., Zhou, J.,
760 Anderson, B., Brekhovskikh, V., and Turner, H.: Biomass burning and pollution aerosol over
761 North America: Organic components and their influence on spectral optical properties and
762 humidification response, Journal of Geophysical Research, 112, D12S18, 2007.

763 Cohen, J. B. and Wang, C.: Estimating global black carbon emissions using a top-down
764 Kalman Filter approach, Journal of Geophysical Research: Atmospheres, 119, 307-323, 2014.

765 Cooke, W., Liousse, C., Cachier, H., and Feichter, J.: Construction of a 1 x 1 fossil fuel
766 emission data set for carbonaceous aerosol and implementation and radiative impact in the
767 ECHAM4 model, Journal of Geophysical Research, 104, 22137-22162, 1999.

768 Curci, G., Hogrefe, C., Bianconi, R., Im, U., Balzarini, A., Baró, R., Brunner, D., Forkel, R.,
769 Giordano, L., Hirtl, M., Honzak, L., Jiménez-Guerrero, P., Knote, C., Langer, M., Makar, P.
770 A., Pirovano, G., Pérez, J. L., San José, R., Syrakov, D., Tuccella, P., Werhahn, J., Wolke, R.,
771 Žabkar, R., Zhang, J., and Galmarini, S.: Uncertainties of simulated aerosol optical properties
772 induced by assumptions on aerosol physical and chemical properties: An AQMEII-2
773 perspective, Atmospheric Environment, 115, 541-552, 2015.

774 Diehl, T., Heil, A., Chin, M., Pan, X., Streets, D., Schultz, M., and Kinne, S.: Anthropogenic,
775 biomass burning, and volcanic emissions of black carbon, organic carbon, and SO2 from
776 1980 to 2010 for hindcast model experiments, Atmospheric Chemistry and Physics
777 Discussions, 12, 24895-24954, 2012.

778 Favez, O., Alfaro, S. C., Sciare, J., Cachier, H., and Abdelwahab, M. M.: Ambient
779 measurements of light-absorption by agricultural waste burning organic aerosols, Journal of
780 Aerosol Science, 40, 613-620, 2009.

781 Feng, Y., Ramanathan, V., and Kotamarthi, V.: Brown carbon: a significant atmospheric
782 absorber of solar radiation?, Atmospheric Chemistry and Physics, 13, 8607-8621, 2013.

783 Fernandes, S. D., Trautmann, N. M., Streets, D. G., Roden, C. A., and Bond, T. C.: Global
784 biofuel use, 1850–2000, Global Biogeochemical Cycles, 21, GB2019, 2007.

785 Flores, J. M., Washenfelder, R., Adler, G., Lee, H., Segev, L., Laskin, J., Laskin, A.,
786 Nizkorodov, S., Brown, S., and Rudich, Y.: Complex refractive indices in the near-ultraviolet
787 spectral region of biogenic secondary organic aerosol aged with ammonia, Physical
788 Chemistry Chemical Physics, 16, 10629-10642, 2014.

789 Forster, P., V. , Ramaswamy, P., Artaxo, T., Berntsen, R., Betts, D. W., Fahey, J., Haywood, J.,
790 Lean, D. C., Lowe, G., Myhre, J., Nganga, R., Prinn, G., Raga, M. S., and Dorland, R. V.:
791 Changes in Atmospheric Constituents and in Radiative Forcing., Cambridge University Press,
792 United Kingdom and New York, NY, USA., 2007.

793 Goldstein, A. H. and Galbally, I. E.: Known and unexplored organic constituents in the earth's
794 atmosphere, Environmental Science & Technology, 41, 1514-1521, 2007.

795 Graber, E. and Rudich, Y.: Atmospheric HULIS: How humic-like are they? A comprehensive
796 and critical review, Atmospheric Chemistry and Physics, 6, 729-753, 2006.

797 Granier, C., Bessagnet, B., Bond, T., D'Angiola, A., Denier van der Gon, H., Frost, G. J.,
798 Heil, A., Kaiser, J. W., Kinne, S., and Klimont, Z.: Evolution of anthropogenic and biomass
799 burning emissions of air pollutants at global and regional scales during the 1980–2010 period,
800 Climatic Change, 109, 163-190, 2011.

801 Hawkins, L. N., Baril, M. J., Sedehi, N., Galloway, M. M., De Haan, D. O., Schill, G. P., and
802 Tolbert, M. A.: Formation of Semisolid, Oligomerized Aqueous SOA: Lab Simulations of
803 Cloud Processing, Environmental science & technology, 48, 2273-2280, 2014.

804 Heald, C., Ridley, D., Kroll, J., Barrett, S., Cady-Pereira, K., Alvarado, M., and Holmes, C.:
805 Contrasting the direct radiative effect and direct radiative forcing of aerosols, Atmospheric
806 Chemistry and Physics, 14, 5513-5527, 2014.

807 Hecobian, A., Zhang, X., Zheng, M., Frank, N., Edgerton, E., and Weber, R.: Water-Soluble
808 Organic Aerosol material and the light-absorption characteristics of aqueous extracts
809 measured over the Southeastern United States, Atmospheric Chemistry and Physics, 10,
810 5965-5977, 2010.

811 Henze, D. K. and Seinfeld, J. H.: Global secondary organic aerosol from isoprene oxidation,

812 Geophysical Research Letters, 33, 09812, 2006.

813 Henze, D. K., Seinfeld, J. H., Ng, N. L., Kroll, J. H., Jacob, D. J., and Heald, C. L.: Global
814 modeling of secondary organic aerosol formation from aromatic hydrocarbons: high-vs. low-
815 yield pathways, Atmospheric Chemistry and Physics, 8, 2405-2420, 2008.

816 Hoffer, A., Gelencsér, A., Guyon, P., Kiss, G., Schmid, O., Frank, G., Artaxo, P., and Andreae,
817 M.: Optical properties of humic-like substances (HULIS) in biomass-burning aerosols,
818 Atmospheric Chemistry and Physics, 6, 3563-3570, 2006.

819 Huang, Y., Wu, S., Dubey, M., and French, N.: Impact of aging mechanism on model
820 simulated carbonaceous aerosols, Atmospheric Chemistry and Physics, 13, 6329-6343, 2013.

821 Iacono, M. J., Delamere, J. S., Mlawer, E. J., Shephard, M. W., Clough, S. A., and Collins, W.
822 D.: Radiative forcing by long-lived greenhouse gases: Calculations with the AER radiative
823 transfer models, Journal of Geophysical Research: Atmospheres (1984–2012), 113, 2008.

824 Jacobson, M. Z.: Global direct radiative forcing due to multicomponent anthropogenic and
825 natural aerosols, Journal of Geophysical Research, 106, 1551-1568, 2001.

826 Jacobson, M. Z.: Isolating nitrated and aromatic aerosols and nitrated aromatic gases as
827 sources of ultraviolet light absorption, Journal of Geophysical Research, 104, 3527-3542,
828 1999.

829 Jaoui, M., Edney, E. O., Kleindienst, T. E., Lewandowski, M., Offenberg, J. H., Surratt, J. D.,
830 and Seinfeld, J. H.: Formation of secondary organic aerosol from irradiated ¥á-
831 pinene/toluene/NOx mixtures and the effect of isoprene and sulfur dioxide, Journal of
832 Geophysical Research, 113, D09303, 2008.

833 Jiang, X., Wiedinmyer, C., and Carlton, A. G.: Aerosols from fires: An examination of the
834 effects on ozone photochemistry in the Western United States, Environmental science &
835 technology, 46, 11878-11886, 2012.

836 Jo, D., Park, R., Kim, M., and Spracklen, D.: Effects of chemical aging on global secondary
837 organic aerosol using the volatility basis set approach, Atmospheric Environment, 81, 230-
838 244, 2013.

839 Kaufman, Y. J., Justice, C. O., Flynn, L. P., Kendall, J. D., Prins, E. M., Giglio, L., Ward, D.

E., Menzel, W. P., and Setzer, A. W.: Potential global fire monitoring from EOS-MODIS, Journal of Geophysical Research, 103, 32215-32238, 1998.

Kim, H. and Paulson, S. E.: Real refractive indices and volatility of secondary organic aerosol generated from photooxidation and ozonolysis of limonene, α-pinene and toluene, Atmos. Chem. Phys., 13, 7711–7723, doi:10.5194/acp-13-7711-2013, 2013.

Kirchstetter, T. and Thatcher, T.: Contribution of organic carbon to wood smoke particulate matter absorption of solar radiation, Atmospheric Chemistry and Physics, 12, 6067-6072, 2012.

Kirchstetter, T. W., Novakov, T., and Hobbs, P. V.: Evidence that the spectral dependence of light absorption by aerosols is affected by organic carbon, Journal of Geophysical Research, 109, D21208, 2004.

Lamarque, J., Bond, T., Eyring, V., Granier, C., Heil, A., Klimont, Z., Lee, D., Mieville, A., and Owen, B.: Historical(1850-2000) gridded anthropogenic and biomass burning emissions of reactive gases and aerosols: methodology and application, Atmospheric Chemistry and Physics, 10, 7017-7039, 2010.

Lambe, A. T., Cappa, C. D., Massoli, P., Onasch, T., Forestieri, S. D., Martin, A. T., Cummings, M. J., Croasdale, D. R., Brune, B., and Worsnop, D. R.: Relationship between oxidation level and optical properties of secondary organic aerosol, Environmental science & technology, 47, 6349-6357, 2013.

Laskin, A., Laskin, J., and Nizkorodov, S. A.: Chemistry of Atmospheric Brown Carbon, Chemical reviews, 115, 4335-4382, 2015.

Laskin, J., Laskin, A., Nizkorodov, S. A., Roach, P., Eckert, P., Gilles, M. K., Wang, B., Lee, H. J., and Hu, Q.: Molecular Selectivity of Brown Carbon Chromophores, Environmental science & technology, 48, 12047-12055, 2014.

Laskin, J., Laskin, A., Roach, P. J., Slysz, G. W., Anderson, G. A., Nizkorodov, S. A., Bones, D. L., and Nguyen, L. Q.: High-resolution desorption electrospray ionization mass spectrometry for chemical characterization of organic aerosols, Analytical chemistry, 82, 2048-2058, 2010.

Liao, H., Henze, D., Seinfeld, J., Wu, S., and Mickley, L.: Biogenic secondary organic

aerosol over the United States: Comparison of climatological simulations with observations, Journal of Geophysical Research, 112, D06201, 2007.

Lin, G., Penner, J. E., Flanner, M. G., Sillman, S., Xu, L., and Zhou, C.: Radiative forcing of organic aerosol in the atmosphere and on snow: Effects of SOA and brown carbon, Journal of Geophysical Research: Atmospheres, 119, 7453-7476, 2014.

Lin, P., Liu, J., Shilling, J. E., Kathmann, S. M., Laskin, J., and Laskin, A.: Molecular characterization of brown carbon (BrC) chromophores in secondary organic aerosol generated from photo-oxidation of toluene, Physical Chemistry Chemical Physics, 2015. 2015.

Liu, J., Scheuer, E., Dibb, J., Ziemba, L. D., Thornhill, K., Anderson, B. E., Wisthaler, A., Mikoviny, T., Devi, J. J., and Bergin, M.: Brown carbon in the continental troposphere, Geophysical Research Letters, 41, 2191-2195, 2014.

Liu, S., Shilling, J. E., Song, C., Hiranuma, N., Zaveri, R. A., and Russell, L. M.: Hydrolysis of organonitrate functional groups in aerosol particles, Aerosol Science and Technology, 46, 1359-1369, 2012.

Lukács, H., Gelencsér, A., Hammer, S., Puxbaum, H., Pio, C., Legrand, M., Kasper-Giebl, A., Handler, M., Limbeck, A., and Simpson, D.: Seasonal trends and possible sources of brown carbon based on 2-year aerosol measurements at six sites in Europe, Journal of Geophysical Research, 112, 2007.

Malm, W. C., Sisler, J. F., Huffman, D., Eldred, R. A., and Cahill, T. A.: Spatial and seasonal trends in particle concentration and optical extinction in the United States, Journal of Geophysical Research, 99, 1347-1370, 1994.

Martin, R. V., Jacob, D. J., Yantosca, R. M., Chin, M., and Ginoux, P.: Global and regional decreases in tropospheric oxidants from photochemical effects of aerosols, Journal of Geophysical Research, 108, 4097, 2003.

McMeeking, G. R.: The Optical, Chemical, And Physical Properties Of Aerosols And Gases Emitted By The Laboratory Combustion Of Wildland Fuels, Dissertation, Department of Atmospheric Science, Colorado State University, Fort Collins, Colorado Fall 2008. Available at: http://chem.atmos.colostate.edu/Thesis/McMeeking%20dissertation.pdf

898 Mischenko, M. I., Travis, L. D., and Lacis, A. A.: Scattering, Absorption, and Emission of
899 Light by Small Particles, Cambridge University Press, UK, 2002.

900 Moise, T., Flores, J. M., and Rudich, Y.: Optical Properties of Secondary Organic Aerosols
901 and Their Changes by Chemical Processes, Chemical reviews, 115, 4400-4439, 2015.

902 Murphy, B. N. and Pandis, S. N.: Exploring summertime organic aerosol formation in the
903 eastern United States using a regional-scale budget approach and ambient measurements,
904 Journal of Geophysical Research, 115, 2010.

905 Myhre, G., Samset, B., Schulz, M., Balkanski, Y., Bauer, S., Berntsen, T., Bian, H., Bellouin,
906 N., Chin, M., and Diehl, T.: Radiative forcing of the direct aerosol effect from AeroCom
907 Phase II simulations, Atmospheric Chemistry and Physics, 13, 1853-1877, 2013.

908 Nakayama, T., Matsumi, Y., Sato, K., Imamura, T., Yamazaki, A., and Uchiyama, A.:
909 Laboratory studies on optical properties of secondary organic aerosols generated during the
910 photooxidation of toluene and the ozonolysis of α-pinene, Journal of Geophysical Research,
911 115, D24204, 2010.

912 Nakayama, T., Sato, K., Matsumi, Y., Imamura, T., Yamazaki, A., and Uchiyama, A.:
913 Wavelength and NO x dependent complex refractive index of SOAs generated from the
914 photooxidation of toluene, Atmospheric Chemistry and Physics, 13, 531-545, 2013.

915 Nguyen, T. B., Lee, P. B., Updyke, K. M., Bones, D. L., Laskin, J., Laskin, A., and
916 Nizkorodov, S. A.: Formation of nitrogen-and sulfur-containing light-absorbing compounds
917 accelerated by evaporation of water from secondary organic aerosols, Journal of Geophysical
918 Research, 117, 01207, 2012.

919 Park, R. J., Jacob, D. J., Chin, M., and Martin, R. V.: Sources of carbonaceous aerosols over
920 the United States and implications for natural visibility, Journal of Geophysical Research,
921 108, 4355, 2003.

922 Park, R. J., Jacob, D. J., Kumar, N., and Yantosca, R. M.: Regional visibility statistics in the
923 United States: Natural and transboundary pollution influences, and implications for the
924 Regional Haze Rule, Atmospheric Environment, 40, 5405-5423, 2006.

925 Park, R. J., Kim, M. J., Jeong, J. I., Youn, D., and Kim, S.: A contribution of brown carbon

926 aerosol to the aerosol light absorption and its radiative forcing in East Asia, Atmospheric
927 Environment, 44, 1414-1421, 2010.

928 Reid, J., Koppmann, R., Eck, T., and Eleuterio, D.: A review of biomass burning emissions
929 part II: intensive physical properties of biomass burning particles, Atmospheric Chemistry
930 and Physics, 5, 799-825, 2005.

931 Rienecker, M. M., Suarez, M. J., Gelaro, R., Todling, R., Bacmeister, J., Liu, E., Bosilovich,
932 M. G., Schubert, S. D., Takacs, L., and Kim, G.-K.: MERRA: NASA's modern-era
933 retrospective analysis for research and applications, Journal of Climate, 24, 3624-3648, 2011.

934 Saleh, R., Robinson, E. S., Tkacik, D. S., Ahern, A. T., Liu, S., Aiken, A. C., Sullivan, R. C.,
935 Presto, A. A., Dubey, M. K., and Yokelson, R. J.: Brownness of organics in aerosols from
936 biomass burning linked to their black carbon content, Nature Geoscience, 7, 647-650, 2014.

937 Schnaiter, M., Gimmler, M., Llamas, I., Linke, C., Jäger, C., and Mutschke, H.: Strong
938 spectral dependence of light absorption by organic carbon particles formed by propane
939 combustion, Atmospheric Chemistry and Physics, 6, 2981-2990, 2006.

940 Srinivas, B. and Sarin, M.: Brown carbon in atmospheric outflow from the Indo-Gangetic
941 Plain: Mass absorption efficiency and temporal variability, Atmospheric Environment, 89,
942 835-843, 2014.

943 Turpin, B. J. and Lim, H. J.: Species contributions to PM2. 5 mass concentrations: Revisiting
944 common assumptions for estimating organic mass, Aerosol Science & Technology, 35, 602-
945 610, 2001.

946 Updyke, K. M., Nguyen, T. B., and Nizkorodov, S. A.: Formation of Brown Carbon via
947 Reactions of Ammonia with Secondary Organic Aerosols from Biogenic and Anthropogenic
948 Precursors, Atmospheric Environment, 63, 22-31, 2012.

949 Wang, X., Heald, C., Ridley, D., Schwarz, J., Spackman, J., Perring, A., Coe, H., Liu, D., and
950 Clarke, A.: Exploiting simultaneous observational constraints on mass and absorption to
951 estimate the global direct radiative forcing of black carbon and brown carbon, Atmospheric
952 Chemistry and Physics, 14, 10989-11010, 2014.

953 Ward, D., Susott, R., Kauffman, J., Babbitt, R., Cummings, D., Dias, B., Holben, B.,
954 Kaufman, Y., Rasmussen, R., and Setzer, A.: Smoke and Fire Characteristics for Cerrado and

955 Deforestation Burns in Brazil: BASE-B Experiment, Journal of Geophysical Research, 97,
956 14601-14619, 1992.

957 Ward, D. E. and Hao, W.: Projections of Emissions from Burning of Biomass Foruse in
958 Studies of Global Climate and Atmospheric Chemistry, Air and Waste Management
959 Association, Vancouver, British Colombia, Canada, 1991.

960 Weber, R. J., Sullivan, A. P., Peltier, R. E., Russell, A., Yan, B., Zheng, M., de Gouw, J.,
961 Warneke, C., Brock, C., and Holloway, J. S.: A study of secondary organic aerosol formation
962 in the anthropogenic-influenced southeastern United States, Journal of Geophysical Research,
963 112, D13302, 2007.

964 Wiedinmyer, C., Akagi, S., Yokelson, R., Emmons, L., Al-Saadi, J., Orlando, J., and Soja, A.:
965 The Fire INventory from NCAR (FINN): a high resolution global model to estimate the
966 emissions from open burning, Geoscientific Model Development, 4, 625-641, 2011.

967 Yang, M., Howell, S., Zhuang, J., and Huebert, B.: Attribution of aerosol light absorption to
968 black carbon, brown carbon, and dust in China–interpretations of atmospheric measurements
969 during EAST-AIRE, Atmospheric Chemistry and Physics, 9, 2035-2050, 2009.

970 Yu, L., Smith, J., Laskin, A., Anastasio, C., Laskin, J., and Zhang, Q.: Chemical
971 characterization of SOA formed from aqueous-phase reactions of phenols with the triplet
972 excited state of carbonyl and hydroxyl radical, Atmospheric Chemistry and Physics, 14,
973 13801-13816, 2014.

974 Zhang, X., Lin, Y.-H., Surratt, J. D., and Weber, R. J.: Sources, Composition and Absorption
975 Ångström Exponent of Light-absorbing Organic Components in Aerosol Extracts from the
976 Los Angeles Basin, Environmental Science & Technology, doi: 10.1021/es305047b, 2013.
977 2013.

978 Zhang, X., Lin, Y. H., Surratt, J. D., Zotter, P., Prévôt, A. S. H., and Weber, R. J.: Light-
979 absorbing soluble organic aerosol in Los Angeles and Atlanta: A contrast in secondary
980 organic aerosol, Geophysical Research Letters, 38, 21810, 2011.

981 Zhong, M. and Jang, M.: Light absorption coefficient measurement of SOA using a UV-
982 Visible spectrometer connected with an integrating sphere, Atmospheric Environment, 45,
983 4263-4271, 2011.

Zhong, M., Jang, M., Oliferenko, A., Pillai, G. G., and Katritzky, A. R.: The SOA Formation Model Combined with Semiempirical Quantum Chemistry to Predict UV-Vis Absorption of Secondary Organic Aerosols, Physial Chemistry Chemical Physics, 14, 9058-9066, 2012.

Table 1. Emission factors (EFs) and calculated parameters used for primary BrC emission estimates. Biomass burning emission is classified for six vegetation types based on the FINN inventory. Here BrC/OC is the mass ratio of BrC to OC emitted from biomass burning and biofuel use.

Source Type	**CO_2 EF [g kg^{-1}]**	**CO EF [g kg^{-1}]**	**MCE**	**OC EF [g kg^{-1}]**	**BC EF [g kg^{-1}]**	**BrC/OC**		
Biomass burning						case1	case2	case3
Boreal Forest	1514	118	0.891	7.8	0.20	0.135	0.093	0.057
Cropland	1537	111	0.898	3.3	0.69	0.946	0.652	0.400
Savanna/Grassland	1692	59	0.948	2.6	0.37	0.189	0.123	0.067
Temperate Forest	1630	102	0.910	9.2	0.56	0.211	0.145	0.088
Tropical Forest	1643	92	0.919	4.7	0.52	0.312	0.213	0.128
Woody Savannah/Shrubland	1716	68	0.941	6.6	0.50	0.123	0.081	0.046
Biofuel[1)]						0.663	0.452	0.271

1) Detailed information is given in Table 2

Table 2. Global biofuel consumption estimates, EFs of OC, and OC biofuel emission estimates for each biofuel category. Base year is 2000.

		Fuelwood	Crop Residues	Dung	Charcoal	Industrial	Total
Biofuel Consumption[1] [Tg]		1351	495	75	39	498	2457
EF [g/kg][2]		2.97[3]	3.3	1.8	1.3	0.91[3]	2.6
OC emission [Gg]		4010.3	1633.5	135	50.7	453.6	6281[4]
BrC/OC	case1	0.653	0.946	0.000	0.000	0.000	
	case2	0.442	0.652	0.000	0.000	0.000	
	case3	0.261	0.400	0.000	0.000	0.000	

1) From Fernandes et al. (2007)
2) From Bond et al. (2004)
3) Global mean value is estimated from Bond et al. (2004)
4) From GEOS-Chem biofuel OC inventory (carbon_200909) by Bond et al. (2007)

Table 3. Global tropospheric budgets of BrC compared to those of OC and BC. Uncertainties are indicated in the parentheses.

Unit : [GgC]	BrC			OC	BC	BrC/OC	BrC/BC
Sources	Biomass burning	3857	(±1689)				
	Biofuel	2965	(±1281)			0.27	1.83
	Anthropogenic SOC	5690				(±0.06)	(±0.43)
	Total	12512	(±2970)	46929	6847		
Wet Deposition	Biomass burning	3169	(±1389)				
	Biofuel	2358	(±1018)			0.28	1.97
	Anthropogenic SOC	5244				(±0.07)	(±0.45)
	Total	10771	(±2407)	38681	5458		
Dry Deposition	Biomass burning	688	(±301)				
	Biofuel	607	(±263)			0.21	1.25
	Anthropogenic SOC	445				(±0.07)	(±0.41)
	Total	1740	(±564)	8272	1397		
Burden	Biomass burning	59	(±26)				
	Biofuel	40	(±18)			0.19	1.84
	Anthropogenic SOC	98				(±0.05)	(±0.41)
	Total	197	(±44)	1021	107		
Lifetime [days]	Biomass burning	5.6	(±0.0)				
	Biofuel	5.0	(±0.0)				
	Anthropogenic SOC	6.3					
	Total	5.8	(±0.1)	7.9	5.7		

Table 4. Extinction efficiencies and SSAs of selected aerosols at 0.4 μm used for calculating photolysis rates in GEOS-Chem. SNA indicates inorganic salt comprised of sulfate, nitrate and ammonium aerosols.

0.4 μm	RH	BrC (Primary)	BrC (Secondary)	OC	BC	SNA
Extinction Efficiency	0%	1.4644	1.2922	1.3933	0.6229	1.2147
	50%	1.6995	1.5645	1.4967	0.6229	1.6566
	70%	1.7873	1.6781	1.5815	0.6229	1.8440
	90%	1.8386	1.7474	1.8485	0.4607	2.2568
	99%	2.2696	2.4390	2.5870	0.4181	2.9655
Single Scattering Albedo	0%	0.5621	0.8683	0.9735	0.1935	1.0000
	50%	0.5474	0.8584	0.9841	0.1935	1.0000
	70%	0.5422	0.8540	0.9873	0.1935	1.0000
	90%	0.5342	0.8480	0.9927	0.3004	1.0000
	99%	0.5412	0.8372	0.9977	0.5233	1.0000

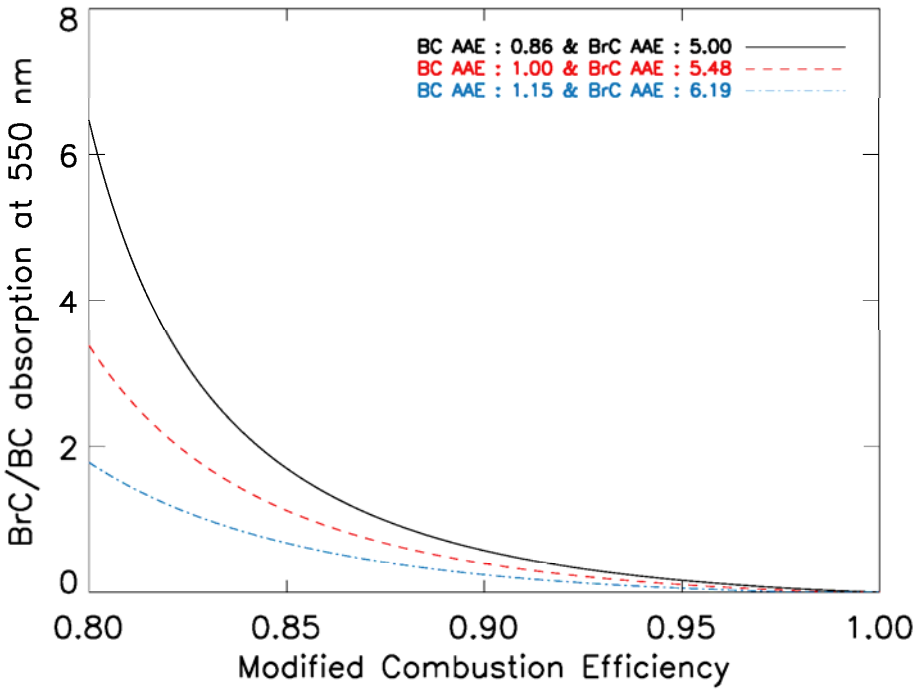

Figure 1. Estimated absorption ratios of BrC to BC at 550 nm as a function of MCE. We assume that the CA absorption is only contributed by BC and BrC absorption. Black solid line indicates case 1, red dashed line represents case 2, and blue dotted line shows case 3.

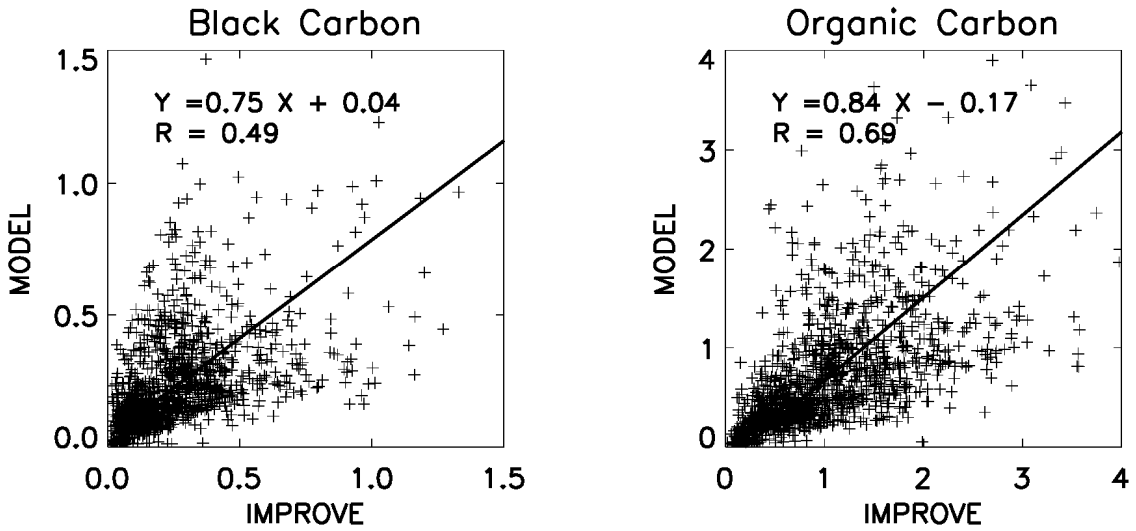

Figure 2. Scatterplot of simulated versus observed BC concentrations (left) and OC concentrations (right). Unit is μgC m^{-3}. Values are monthly means for 2007. Regression equations and correlations are shown inset. Regression is computed with reduced major axis (RMA) method.

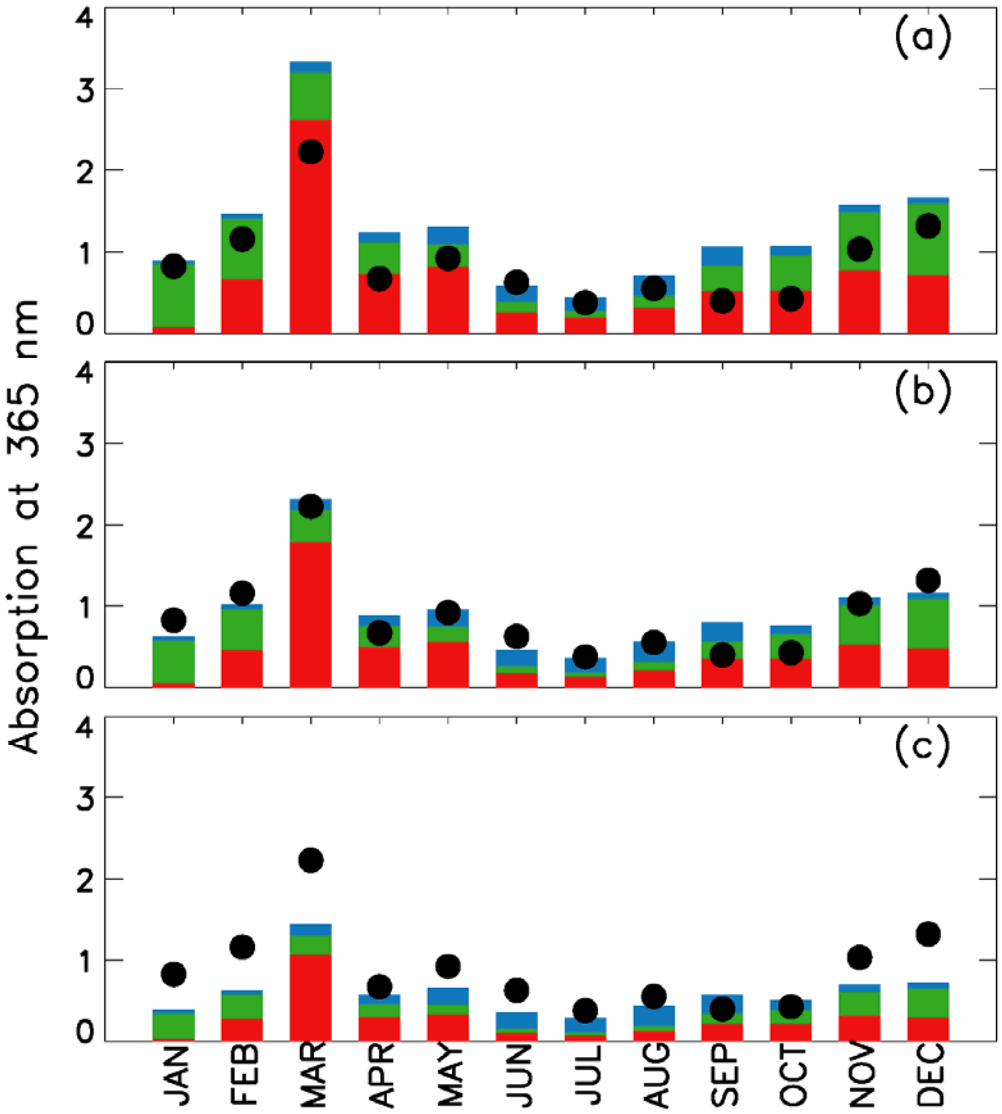

Figure 3. Simulated versus observed monthly mean light absorption at 365 nm by water soluble BrC over the southeastern US in 2007. Unit is Mm^{-1}. Black circles denote observations, and bar graphs indicate model results for each source: biomass burning (red), biofuel (green), and SOA (blue). Each panel shows the comparisons with different emission estimate cases – (a) case 1, (b) case 2, and (c) case 3.

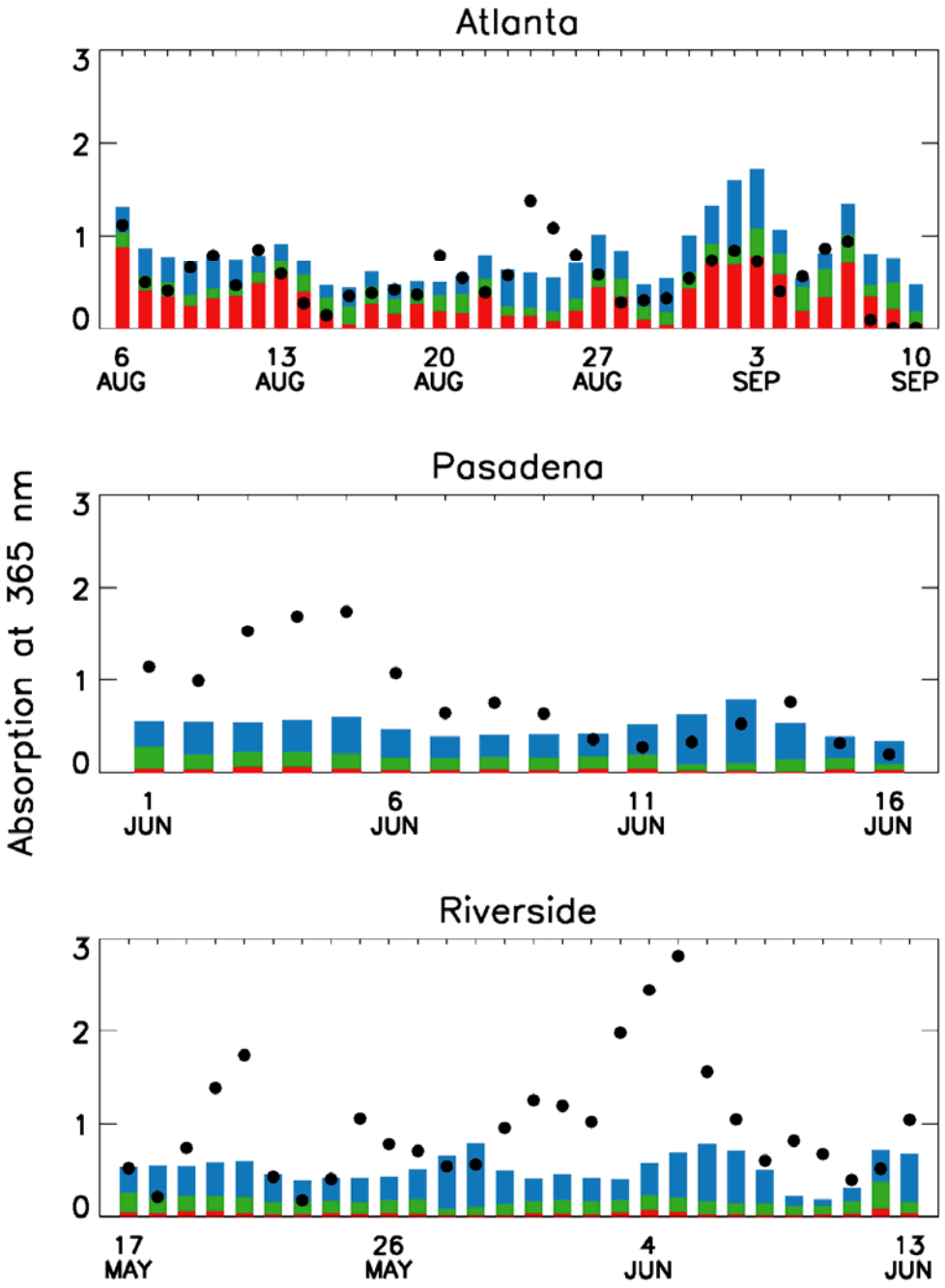

Figure 4. Simulated versus observed daily mean light absorption at 365 nm by water soluble BrC over the US in 2010. Unit is Mm^{-1}. Black circles denote observations and bar graphs indicate model results for each source – biomass burning (red), biofuel (green), and SOA (blue).

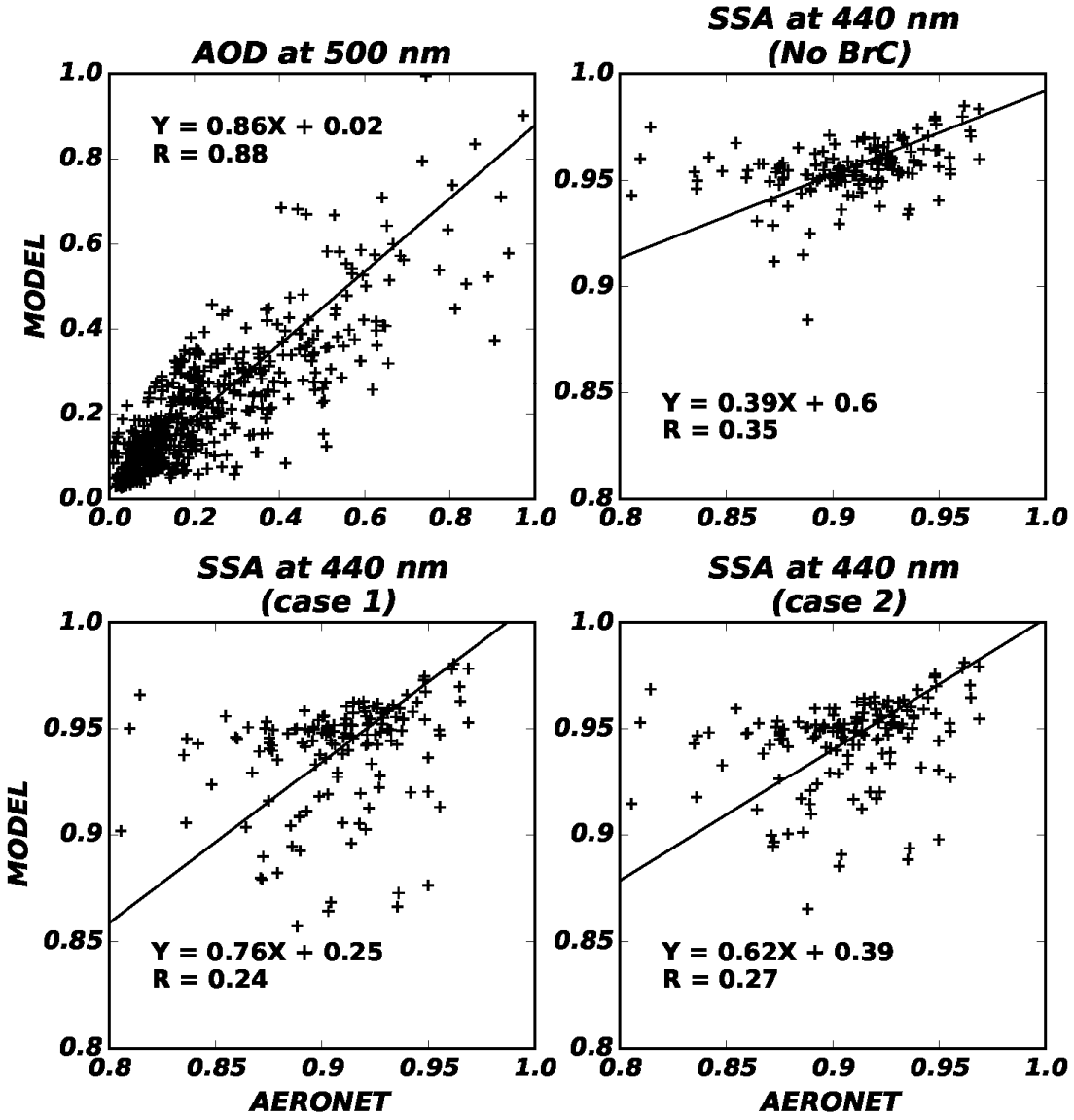

Figure 5. Scatterplots of simulated versus observed AOD at 500 nm (upper left), SSA at 440 nm without BrC (upper right), SSA at 440 nm with BrC of case 1 (lower left), and SSA at 440 nm with BrC of case 2 (lower right) for 2007. Reduced major axis regression is shown along with the regression equation and R. Each point indicates monthly averaged AOD or SSA when the number of observation is greater than 10 days.

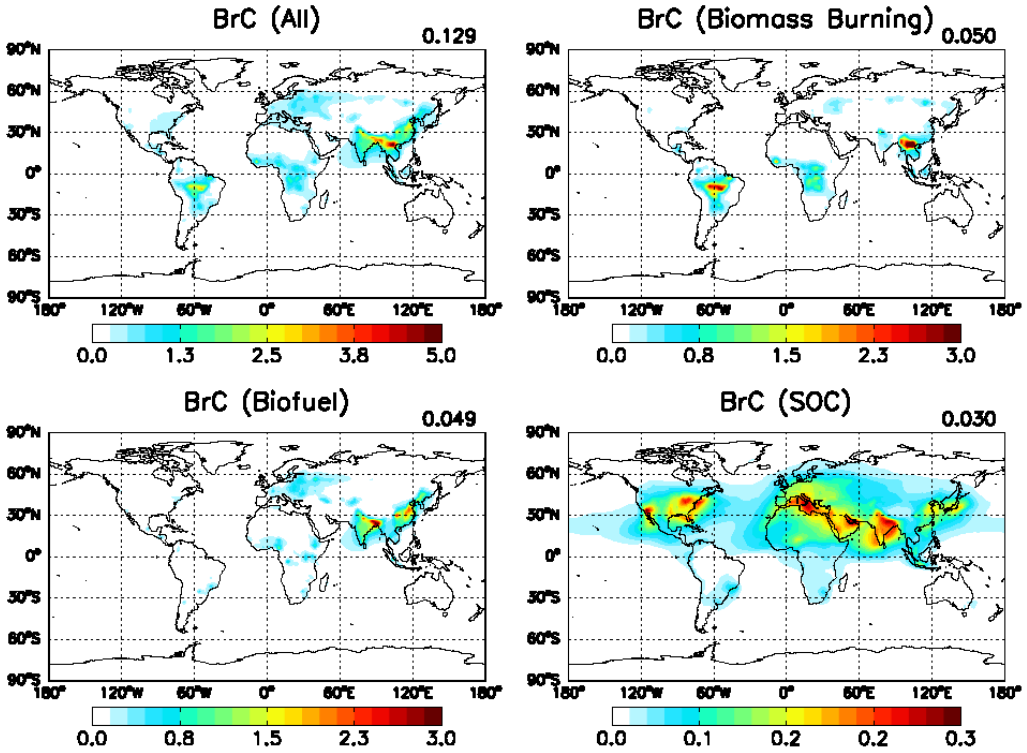

Figure 6. Annual surface map of total BrC (top left) and BrC from three source categories: biomass burning (top right), biofuel (bottom left), and SOC (bottom right). Mean values are presented in the upper right corner of each panel. Unit is μgC m^{-3}.

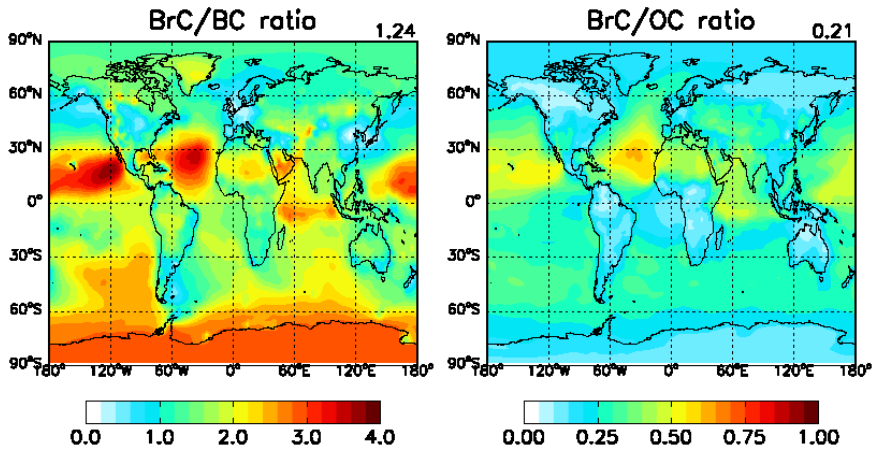

Figure 7. Annual mean ratios of BrC to BC (left) and OC (right) in surface air. Global mean values are presented in the upper right corner of each panel.

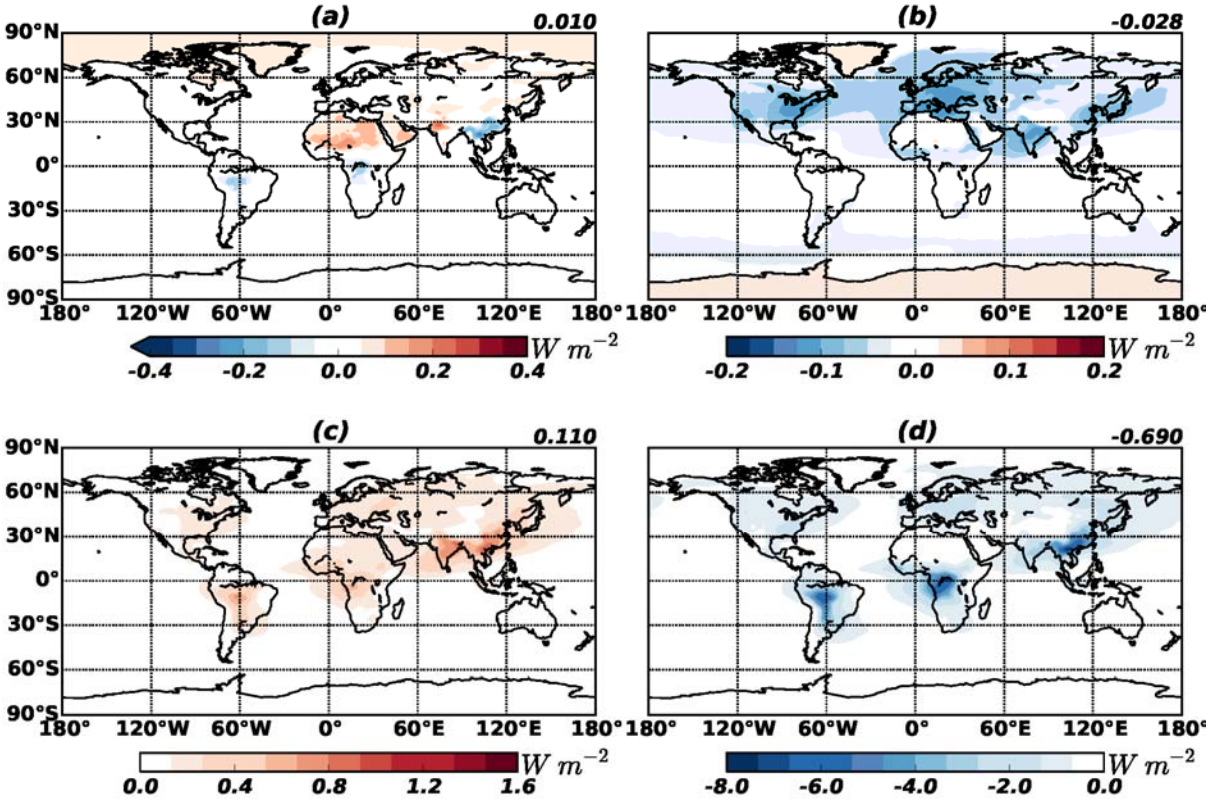

Figure 8. DRE of BrC at the top of the atmosphere. Upper panels are for radiative effect of BrC from primary sources (a) and from secondary sources (b). The DRE increase of OC owing to the absorption of BrC is shown in (c) (i.e. the DRE of OC with absorbing BrC minus the DRE of OC including BrC as scattering OC, which is typically assumed in previous studies). Radiative effect of total OC (BrC is assumed to be scattering OC) is represented in (d). The 70°S–70°N averages are shown in the upper right corner of each panel.

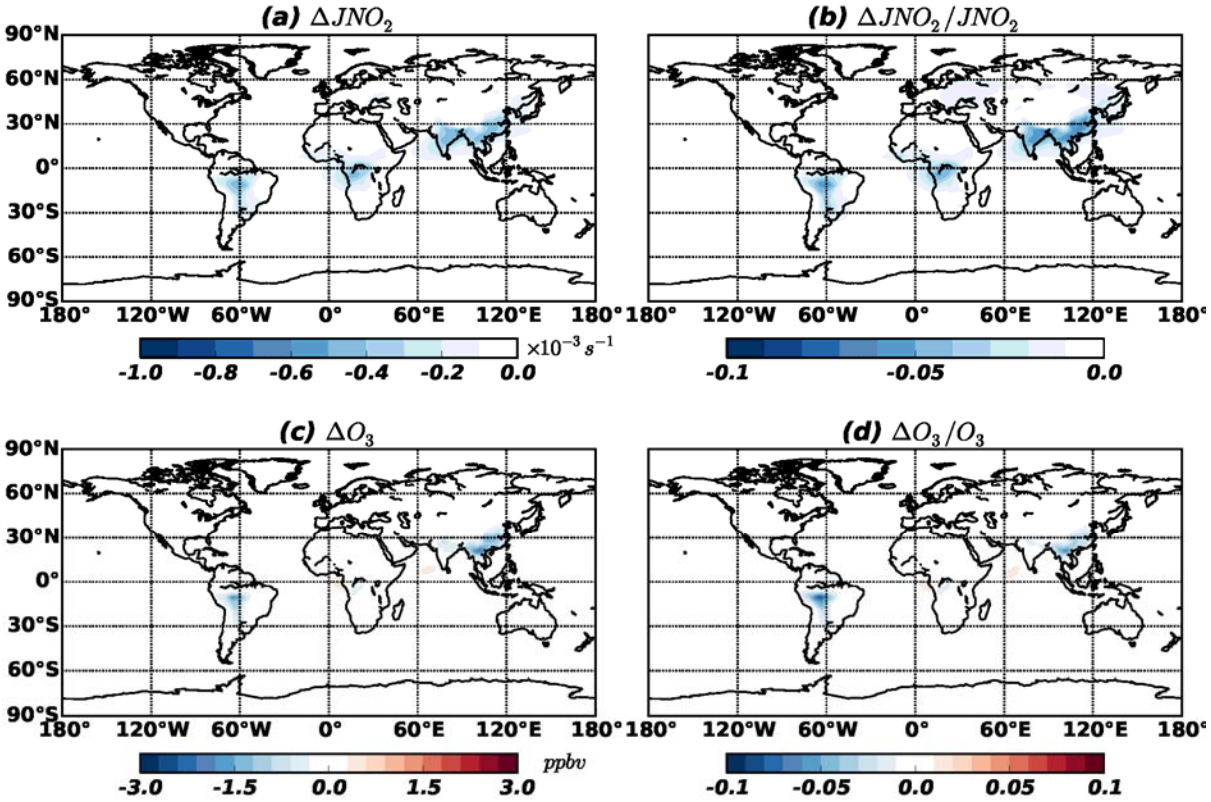

Figure 9. Changes in annual NO_2 photolysis rate (a,b) and O_3 concentration (c,d) at the surface due to BrC absorption.